SYSTEM-LEVEL INTEGRATION AND PACKAGING OF NANOSENSOR EMBEDDED MICROFLUIDICS WITH ELECTRICAL READOUT

by
OĞUZ MUSTAFA ALBAYRAK

Submitted to the Graduate School of Engineering and Natural Sciences
in partial fulfilment of
the requirements for the degree of Master of Science

Sabancı University
July 2023

SYSTEM-LEVEL INTEGRATION AND PACKAGING OF NANOSENSOR
EMBEDDED MICROFLUIDICS WITH ELECTRICAL READOUT

Approved by:

Assoc. Prof. Dr. MURAT KAYA YAPICI …………………………..
(Thesis Supervisor)

Prof. Dr. DEVRİM GÖZÜAÇIK …………………………………..

Asst. Prof. Dr. ÖMER CEYLAN …………………………………..

Approval Date: July 26, 2023

ABSTRACT

SYSTEM-LEVEL INTEGRATION AND PACKAGING OF NANOSENSOR EMBEDDED MICROFLUIDICS WITH ELECTRICAL READOUT

OĞUZ MUSTAFA ALBAYRAK

ELECTRONICS ENGINEERING M.Sc. THESIS, 2023

Thesis Supervisor: Assoc. Prof. Dr. MURAT KAYA YAPICI

Keywords: integration, nanosensor, microfluidics, electrical readout, packaging

The development of innovative biosensor technologies necessitates the smooth integration of electronic and microfluidic components. Researchers often find themselves expending significant effort and financial resources in the pursuit of parameter optimization, all the while experiencing challenges with complex system designs. Unfortunately, literature in this domain often suffers from a lack of comprehensive methodological elucidation. In the present thesis, the focus is on designing the auxiliary features that make chip's sensing region useful. In particular, the design and fabrication of electrical readout connections to a sensitive region comprising parallel arrangement of $100\,\mu m$ long nanoscale sensing elements and its interfacing to a microfluidic analyte are studied by utilization of the most commonly used materials of microfluidics studies, namely PDMS and SU-8. Each parameter is thoroughly investigated by considering the microfluidic channel dimensions, geometries, and connection schemes to enhance the overall design's precision. The outcome catalogue can be utilized as a generic tool for developing lab-on-a-chip devices for point-of-care applications, particularly in the field of disease diagnostics.

ÖZET

NANOSENSÖR GÖMÜLÜ MİKROAKIŞKANLARIN ELEKTRİKSEL OKUMA İLE SİSTEM DÜZEYİNDE ENTEGRASYONU VE PAKETLENMESİ

OĞUZ MUSTAFA ALBAYRAK

ELEKTRONİK MÜHENDİSLİĞİ YÜKSEK LİSANS TEZİ, 2023

Tez Danışmanı: Assoc. Prof. Dr. MURAT KAYA YAPICI

Anahtar Kelimeler: entegrasyon, nanosensör, mikroakışkanlar, elektriksel okuma, paketleme

Yenilikçi biyosensör teknolojilerinin geliştirilmesi, elektronik ve mikroakışkan bileşenlerin sorunsuz bir şekilde entegre edilmesini gerektirmektedir. Araştırmacılar genellikle kendilerini parametre optimizasyonu arayışında önemli çaba ve mali kaynaklar harcarken bulurken, bir yandan da karmaşık sistem tasarımlarıyla ilgili zorluklarla karşılaşmaktadır. Ne yazık ki, bu alandaki literatür genellikle kapsamlı metodolojik açıklama eksikliğinden muzdariptir. Bu tezde, çipin algılama bölgesini kullanışlı hale getiren yardımcı özelliklerin tasarlanmasına odaklanılmaktadır. Özellikle, 100 um'lik bir hassas bölgeye elektriksel okuma bağlantılarının tasarımı ve imalatı ve bunun mikroakışkan bir analitin yüklenmesi ile, mikroakışkan çalışmalarında en yaygın kullanılan malzemeler olan PDMS ve SU-8 kullanılarak incelenmiştir. Her bir parametre, genel tasarımın hassasiyetini artırmak için mikroakışkan kanal boyutları, geometrileri ve bağlantı şemaları dikkate alınarak kapsamlı bir şekilde incelenmiştir. Elde edilen katalog, özellikle kanser teşhisi alanında olmak üzere, çip-üzerinde-laboratuvar-cihazlarında hasta başında test uygulamalarında geliştirmek için genel bir araç olarak kullanılabilir.

ACKNOWLEDGEMENTS

Common sense is the least common…

Sağduyu en az duyulandır…

TABLE OF CONTENTS

LIST OF TABLES

LIST OF FIGURES

LIST OF ABBREVIATIONS

lab-on-a-chip	LOC
point-of-care	PoC
micro-electro-mechanical systems	MEMS
micro-total analysis systems	μTAS
organic electrochemical transistors	OECT
solution-gated organic transistors	SGOFET
organic charge modulated field effect transistors	OCMFET
organic field effect transistors	OFET
conductive polymer	CP
electrical double layer	EDL
electron beam lithography	EBL
research and development	R&D
metallic nanowires	NWs
polymethyl-methacrylate	PMMA
lower molecular weight	LMW
high molecular weight	HMW
polymerase chain reaction	PCR
Human Genome Project	HGP
Reynolds number	*Re*
Péclet number	*Pe*
poly(dimethylsiloxane)	PDMS
isopropyl alcohol	IPA
silanol	SiOH
stereo-lithographically	SLA
source/measure units	SMUs
physical vapor deposition	PVD
Fused deposition modelling	FDM
device under test	DUT
current	I
resistance	R
high force	HF
low force	LF
high/low sense	HS/LS
dielectrophoresis	DEP
positive DEP	p-DEP
negative DEP	n-DEP
Clausius-Mossotti	CM
red blood cells	RBC

1. INTRODUCTION

Interdisciplinary efforts put in bioscience throughout decades cumulated vast amount of knowledge and know-how, leading to significant advancements in detection, purification, and quantification of biological markers, especially those that are anticipatedly useful in medical disease diagnostics and/or treatment of terminal diseases. Ever-evolving biotechnological practices around biomarker sensing aiming higher sensitivity, specificity, and throughput, have achieved their most recent advancements in parallel with the latest milestones in accompanying microfluidic systems.

Historically, first microfluidic applications such as inkjet printing were utilizing silicon wafers [1]. Over time, the use of glass began to attract interest, by virtue of showing similar properties to silicon at lower costs with the additional advantage of optical transparency that enable development of optic based applications [2]. After introduction of poly(dimethylsiloxane) (PDMS) as a biocompatible, soft, flexible, optically transparent, and affordable elastomer to the microfluidics world, its use became widespread in a short time in plethora of biological [3] and chemical [4] applications. Owing to its low surface energy characteristics, PDMS fills in very small features upon casting over a mold of desired structures, providing quick and easy replication of even submicron features. For most microfluidic applications pertaining structures not smaller than dozens of micrometers, use of PDMS can eliminate cleanroom requirements. Furthermore, elastic nature of the material enables leakage-free and reversible sealing for channels by simple mechanical attachment on flat surfaces, insomuch as permanent bonding through various surface modification techniques such as plasma treatment [5] or bonding by curing agent [6]. Another common material used in microfluidics is SU-8, developed by IBM towards the millennium. SU-8 is a negative tone photoresist material, that can be directly utilized as lithographically patterned channel structures upon spin

coating. Due to its high viscosity characteristics, it provides structural layers of thicknesses, varying from tens of microns up to 1200 µm [7], which is tunable by its polymeric compounds and spin-coating speed.

Along with PDMS and SU-8, exploitation of various novel materials for fluid manipulation at the microscale by integrating laboratory functions onto a single chip or device led to formation of Lab-on-a-Chip (LoC) concept. Meanwhile miniaturization trend in electronics paved the way through integration of diverse functionalities in small packaging domains, which enabled performing medical diagnostics or testing at or near the location where patient care is provided, such as a doctor's office, a clinic, or even at home; in a nutshell, at the Point-of-Care (PoC).

1.1. Background on Lab-on-a-Chip Systems & Point-of-Care Devices

According to marketdataforecast.com report [8], LoC market size is expected to exceed 9.8 billion USD by 2028 which corresponds to a 8.9% mean annual growth rate in five years. The demand is increasing with proliferation of biotechnology research that brings the availability and adoption of the microchips in diagnostics and testing devices used in healthcare instead of large and costly equipment that require trained personnel. Increasing research efforts also increase the demand for instruments like microarrays, microfluidics, tissue biochips for drug discovery and replacement of in-vivo tests. Supplementary software, such as machine learning algorithms optimized for counting and quantification of biological samples by image processing, are also strongly demanded. Regionally, North America, Asia Pacific and Europe have the largest market shares, followed by emerging economies with a high growth rate.

Traditional diagnostic methods rely on complex lab equipment and skilled operators, leading to lengthy waiting times, often lasting several days, and invasive techniques. Miniature lab-on-chip (LoC) devices provide several benefits over traditional instruments. These include accurate liquid control, reduced sample usage, faster reaction times, and portability. With this technology, it is possible to achieve precise liquid flow control and sensitive detection of analytes. The applications of this approach are diverse,

including PoC diagnostics, research, chemistry, monitoring, and biohazard detection. The LoC technologies are offering a potential for full covering of a diagnostic system including sample loading then measurement followed by a more reliable quantitative or qualitative test result [9]. As a result, the demand for PoC solutions becomes increasingly important in a world with a growing population. PoC testing systems provide user-friendly instruments that can be operated by non-specialized personnel in various locations, including offices, field incidents, ambulances, and hospitals. Rapid test results at the point-of-care facilitate immediate treatment. Also, enhanced accuracy and quantitative data compared to laboratory analysis would reduce the risk of misdiagnosis and improper treatment. One of the most known commercially available PoC devices are electrochemical glucose test strips designed for diabetes self-monitoring and lateral-flow assay strips frequently employed in pregnancy testing. However, these devices encounter quantitative and mechanical limitations such as precise glucose level measurement and the determination of positive/negative test outcomes that might be leading to unreliable results.
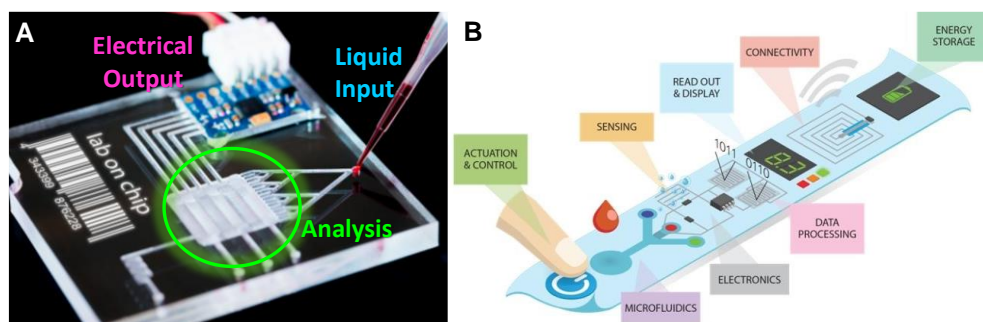
Figure 1. LoC & PoC concepts.

(A) An example for LoC device with liquid input, on-chip analysis module and integrated electrical readout (image taken from Polytec GmbH website) (B) Visualization of a PoC device with various functional modules, image taken from [10].

A comprehensive review highlights the primary obstacles in utilizing LoC devices, such as the sealing techniques required for bonding with various substances like plastics and adhesive layers. Furthermore, the study points out the difficulty of integrating fluidic interfaces and electrical connections, including the methods for interconnection [3].

Mitri et al. introduce a new bonding method of SU8 that has proven to be highly effective [11]. This process involves exposing patterned SU-8 films to light with a wavelength of 254 nm (Figure 2). This opens the residual epoxy rings in the resin, allowing them to be brought into contact, resulting in chemical bonding. This process successfully overcomes the challenge of bonding patterned SU8 layers at lower temperatures.
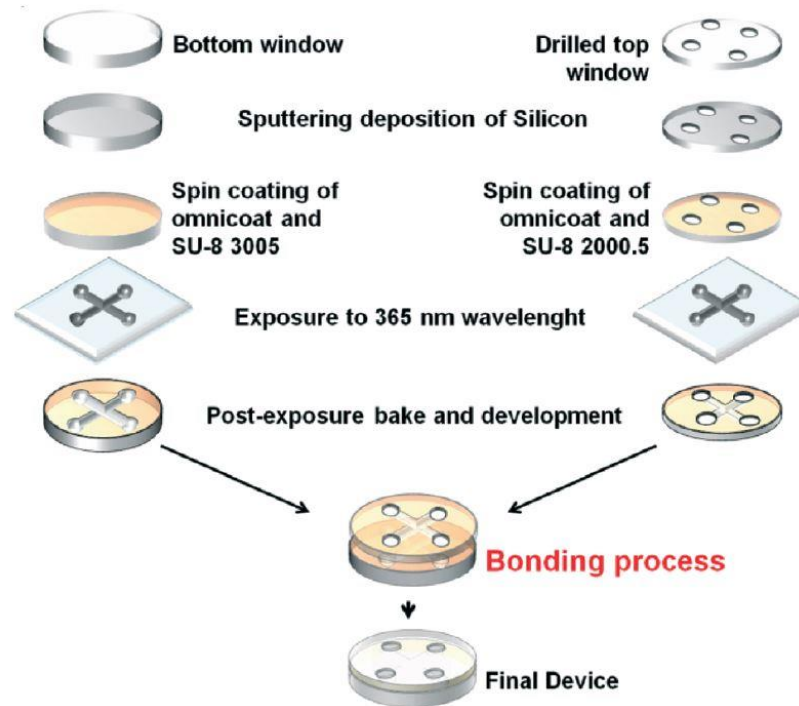
Figure 2. Schematic of the fabrication and bonding process for a fully closed SU-8 microfluidic device, image taken from Mitri et al. [11].

Besides these, Azizipour et al. reviewed the evolution of biochip technology and systems, also referred to as LoC or micro-total analysis systems (µTAS) together with current Organ-on-a-Chip (OoC) platforms for lung, cardiovascular, brain, liver, kidney, gut and skin [12]. In the article, beyond the research, companies and current applications for diagnostics, therapeutics, drug delivery, biosensors and tissue engineering are reviewed and future perspectives for point-of-care are discussed. A list of selected PoC diagnostic devices with respect to their applications (HIV/AIDS, cardiovascular disease, flu, pathogens, respiratory infections, etc.), sample types (whole blood, plasma, sputum, urine, nasal/vaginal/rectal swabs, etc.), signal detection types (fluorescence, electrochemical, colorimetric, optical, etc.) and structural features (disposable cards, capillary microfluidic test strip, etc.) is given. Among the reported OoC devices, there is a lack of monitoring microenvironmental parameters and drug responses over time. To

overcome this issue, Aleman et al suggested the combination of electrochemical microelectrodes with the microfluidic chip [13]. The electrodes consist of patterning Au working electrode (WE), Au counter electrode (CE), and Ag reference electrode (RE) on a glass substrate. A versatile method for capturing protein biomarkers in cell culture medium and a blocking step to eliminate nonspecific binding of nontarget proteins using the electrochemical electrodes is reported in this study. After ensuring the protein selectivity of the electrodes, the regeneration of antibody and aptamer-based biosensors for soluble antigens can be achieved with these electrodes (Figure 3). On the other hand, they created a microfluidic chip that includes a microchamber and microchannels with pneumatic valves for precise liquid routing. The chip is composed of three layers that are bonded together using plasma treatment. Additionally, a thin PDMS membrane serves as a pneumatic valve between the layers. To ensure complete pneumatic sealing, the square microfluidic channel on the bottom layer has been transformed into a convex hemicylindrical shape. Furthermore, their study comprehensively protocolized constructing scheme of a fully integrated microfluidic breadboard complex with electrochemical detection capabilities (Figure 3) for several biomarkers, which makes it a valuable guideline for OoC applications.
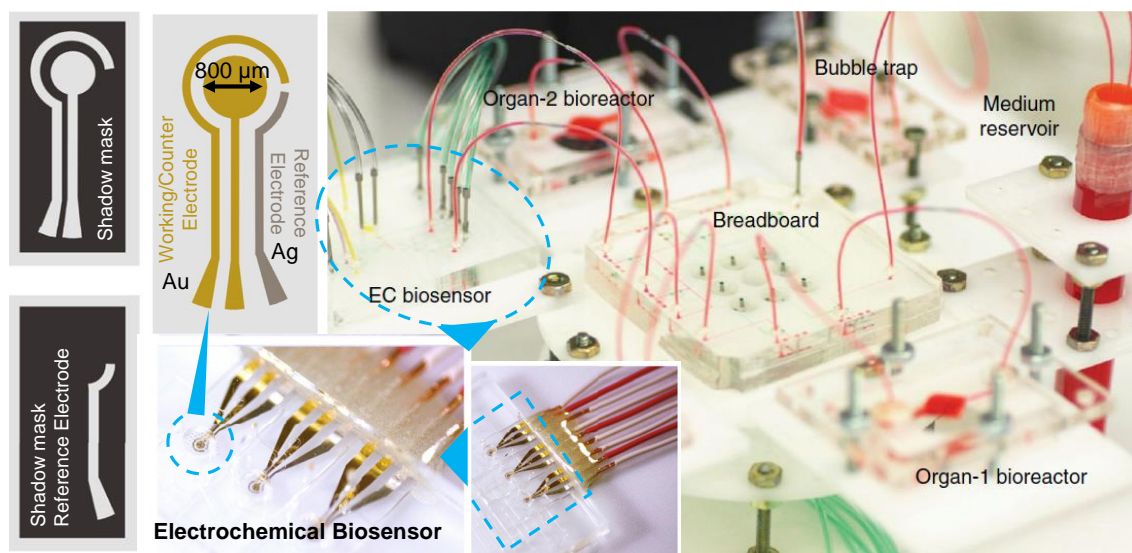
Figure 3. Photograph showing multisensor-integrated multi-organ-on-chips platform. (right), with electrochemical affinity sensor (middle) with Au WE, Au CE, and Ag RE-microfabricated through two shadow masks (leftmost). (Image taken from [13])

Enhancing the performance of organic FETs can be achieved by leveraging sophisticated microfluidic systems featuring superior designs. A plethora of research studies have delved into this realm, and there is potential for further exploration of integrating logic gates with intricate systems utilizing suitable microfluidic systems in the organ-on-chip curriculum. A study by Spanu et al. reviews organic field effect transistors, more specifically organic electrochemical transistors (OECT), solution-gated organic transistors (SGOFET) and organic charge modulated field effect transistors (OCMFET) [14]. It is mentioned that organic FETs (OFET) are being deeply studied and optimized in time. Principles and schematics of these semiconductors (similar to typical FETs but fabricated with biocompatible materials and arrangements), the active channel of the device is a semi-conductor between a source and a drain channel that builds up an electrical switch conditionally separated by a certain threshold voltage, either being an enhancement or depletion mode device, depending on the design. Interfacing cells from their viable environment to the macro-world is possible by constructing logical gates by combination of these transistors. First devices using stimulation by electrical fields had limitations such as high voltage requirement and unstable liquid environment, which make them inappropriate for cell sensing. However, with different types of OFETs proposed in the last decade high transconductance, high sensitivity and low operating voltages (below 1V) are possible and the change in transconductance by perturbation by presence and/or activation of cells can be sensed. As the advancements propagate with novel configurations, these organic transistors enable variety of promising assessment and monitoring methods for cellular activities, sub-tissue cellular cultures and cytotoxicity studies in vitro and in vivo. Furthermore, studies on 3D cellular structures hold great potential to mimic living organisms [15]. Therefore, they stand out as a promising approach for creating complex artificial living systems, which, in theory, can be operated on a biologically driven rule-based algorithm.

1.2. Biomarker Sensing Mechanisms and Limitations

One of the common application areas for PoCs are biomarker quantification [16]. These markers provide measurable parameters for a person's state of health, some could be

harbinger of a disease while others could indicate the level of well-being [17]. They can be harvested from various sources on the body such as urine, saliva, cerebral fluid, or blood plasma. Blood plasma is heavily studied as it carries a rich source of information, and has a wide availability from different parts of the body [18]. Thanks to this interest around blood plasma study, there are now well-established methods for blood biomarker detection such as gel-electrophoresis, electrochemical assays, colorimetric assays, flow cytometry, polymerase chain reaction (PCR) and infrared (IR) spectroscopy [19]. Gel electrophoresis demonstrated to be a valuable technique for separation of charged particles like nucleic acids and proteins with an application of a current through gel medium [20]. There is a trade-off with that comes with the utilization of the gel, though it allows for a medium for current application; analytes are usually stuck in the gel and need to be re-harvested for further analysis. This decreases the throughput of the technique while increasing the labour need [19]. Electrochemical assays rely on utilization of ion-sensitive electrodes for electrolyte detection, molecules such as glucose and creatine can be detected through their interaction with a reporting enzyme which creates electrically detectable change. It provides fast and biofluid compatible detection method, only drawback being that untargeted molecules could interfere with the electrodes [21]. Colorimetric assays follow a similar principle, this time though interaction of targeted electrolyte with the enzymes ends up with creation of hydrogen peroxide which colours a colourless substrate [19]. Flow cytometry, on the other hand, is directly used for cell detection and helpful in the cases that existence of some cells could be considered as biomarkers. Its fundamental principle is based on passing/flowing analyte cells through laser focused areas as resulted scattering and fluorescence is studied [22]. It inherently works for big particles (cell-sized) and could suffer from background noise [23]. Fourier transform IR spectroscopy (FTIR) is used for detection of incredibly diverse variety of molecules such as proteins, carbs to different plasmas [24]. It is still in need of improvement, however; since in vivo analysis is lacking and sensitivity levels need to be increased.

PCR could be the most famous of these methods as it's heavily used in nucleic acid detection, in which selected DNA sequences could be amplified immensely up to billions of copies [25]. Drawbacks of PCR though are again related to expense of its equipment, and reagents like all the other previously mentioned methods.

Although postulation of the memristor as the fourth fundamental element of electronics is relatively outdated, not until 2011 a memristive device was reported to be used for biosensing [26]. Since then, it has been drawing attention with remarkable outcomes in biomarker sensing applications [27]. Detecting biomarkers with memristors is similar to FETs, where binding between bioreceptors and biological analytes induces a change in conductance. However, in memristors, this transformation (known as bio-functionalization) involves the attachment of charged components, such as antibodies, to the device's surface, resulting in an interruption in a logarithmic current-voltage curve. Attaching antibodies to the surface of a memristor induces a modification in its conductance, leading to an alteration in the voltage gap as compared to its initial condition. Most memristive devices come onto stage in the form of semiconductor nanowires (NWs) [28], for which some microfluidic and electrical integration strategies are presented in the literature ().
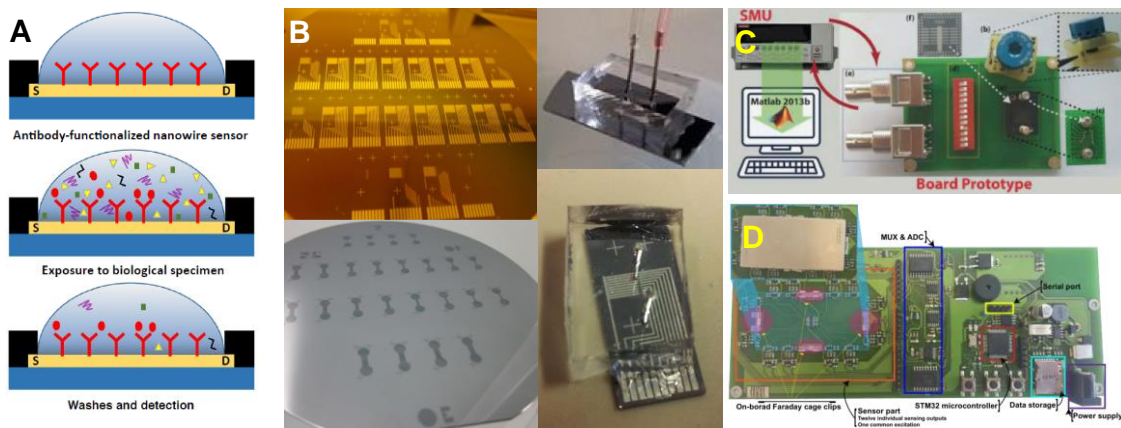
Figure 4. Studies on nanowire-based memristive sensors.

(A) Operating principle of a semiconductor NW sensor [28]. (B) First memristive biosensor which is integrated to microfluidics [29]. (C) Electronic measurement interface for SiNW memristive biosensor [30]. (D) A prototype memristive biosensor board [31].

One common area of improvement for all these methods could be found on their sensor interfaces which regulates the interaction of sensor with the analytes and translates the sensor data.

1.3. Motivation of this study

Developments in micro-electro-mechanical systems (MEMS) and processing technologies unleashed the potential of many applications, especially in bioscience by enabling precise control over very small environments down to scales that are compatible with sizes smaller than an individual cell. Development of a sensor/actuator for a low quantity analyte or detection/quantification of a rarefied substance in large volumes necessitates such downsizing of the sample-sensor/actuator interface along with an integrated read-out/manipulation circuit to achieve fast and precise analysis for biological markers such as proteins, nucleotides, hormone, and pathogen detection, where a holistic approach for system-level integration of the key sensing unit to microfluidics in synchrony with electronics gains importance.

This work aims to provide a universal guideline for integration of any biomarker sensor with its microfluidic channels and electrical readout. After discussing the fundamental points to consider, method development procedure based on a structure with the sensitive length of 100 µm is studied and proof-of-concept physical implementations are presented.

This thesis is organized as follows: Chapter 2 discusses the integration methodology of microfluidics, starting from biochip fabrication. Fabrication section is followed by discussion of microfluidics integration first by focusing on generic design considerations, then by different material-oriented methods, where utilization PDMS and SU-8 are studied and practical results from several applications were presented to accompany. This chapter is concluded by presentation of microfluidic interfacing studies based on these applications. Chapter 3 discusses electrical integration methods and readout mechanisms, together with system-level integration schemes around design studies realised within this framework. In Chapter 4, functional testing and application scenarios are presented. The applications include measurement-guided microfluidic integration progress optimization and a proof-of-concept di-electrophoresis based separation application in simulation environment. Finally, a conclusion is provided which outlines a guideline and the general

constraints to be addressed while optimizing sensor to system integration.

It's believed and hoped that design flow presented here could inspire faster turnaround times for engineers working on different biomarker sensor systems and become backbone for similar ones.

2.   MICROFLUIDICS INTEGRATION METHODOLOGY

Implementation of detection and/or quantification of biological analytes through direct electrical measurement necessitates utilization of structures in comparable dimensions. For that reason, Au nanowires connected to the micro-scale measurement pads are designed and fabricated as detailed in Section 2.1. Afterwards, experimental studies on several approaches on microfluidic channel design and integration are presented in Section 2.2. Additionally, the design development process of the chip layout in coalescence with the electrical measurement setup, experiments conducted for establishment of electrical integration and verification of repeatability by resistance measurement analyses after fabrication and microfluidics integration steps are concisely discussed from the microfluidics perspective and detailed in the next chapter.

2.1. Biochip Fabrication

Electron beam lithography (EBL) is a highly effective technique for precise nanometer-scale patterning. It serves as a tool mostly for low-volume research and development (R&D) prototyping, because of high-cost and slow processing characteristic of direct writing. EBL is employed with pattern transferring methods like etching or lift-off, among which lift-off is often preferred in research due to its simplicity, cost-effectiveness, and safety. Unlike lift-off, dry etching methods involve complex instruments and poisonous gases, whereas wet etching incorporate highly reactive chemistries with the requirement of handling under fume hood and other safety precautions, nonetheless the etching process itself interweave uncertainties such as etchant compatibility, selectivity, and high dependency on process conditions. Lift-off offers a convenient and "undercut-free" pattern transfer process, making it especially useful for metallic multilayer compositions

and unique alloys where compatibility to or selectivity of etchants may be unsettled. Fabrication of nanometallic features below 100 nm with lift-off-based EBL patterning is extensively studied by Şahin [32]. A production scheme optimized in his work has been adopted for fabrication of the nanowire settings, as the central measurand of this study.

The process flow for fabrication of the metallic nanowires (NWs) on a glass substrate starts with spin-coating of two overlapping polymethyl-methacrylate (PMMA) layers as positive tone resist. Bottom layer is the PMMA with lower molecular weight compounds (LMW-PMMA), expediting higher development rates upon exposure to beam of electrons, than the top layer of high molecular weight PMMA (HMW-PMMA). This bilayer structure enables undercut profiling of the exposed pattern in the resist upon development, which is required to provide discontinuity in the subsequently deposited metallic layer inside the developed pattern and on the resist layer for a complete lift-off. Cross sectional representation of the fabrication process flow and images of products by Şahin are presented in Figure 5.
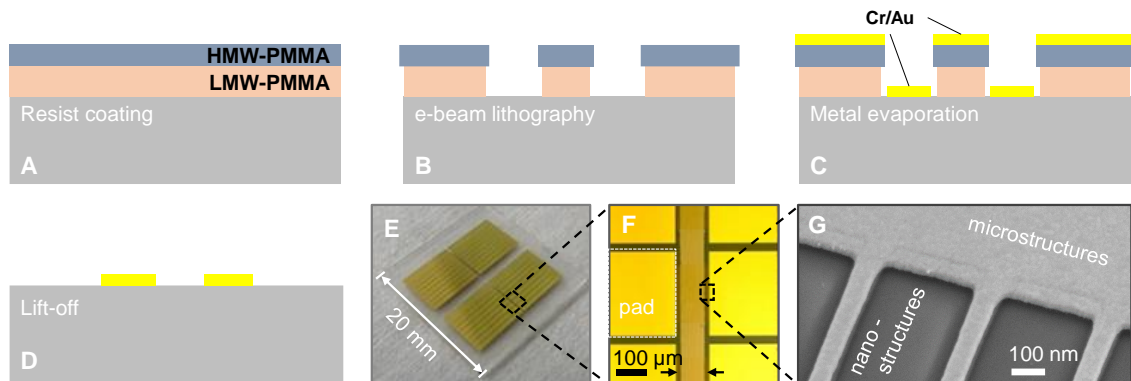
Figure 5. lift-off based fabrication scheme of nanowires.
(A) Spin-coating PMMA bilayer, (B) resist patterning by e-beam lithography and development, (C) deposition of Cr/Au stack by physical vapour deposition, and (D) lift-off. (E) Photograph of a produced chip with large contact pads. (F) NW region centred optical microscopy image. (G) SEM image showing the merging point of the NWs and the pad.

Keeping up with the same production scheme, several layout designs were generated with a bottom-up approach to achieve NW's interfacing to microfluidics and system-level

integration to electrical readout. As a rule of thumb, downsizing of the devices is favoured for high throughput and low-cost fabrication. The lowest dimensional limits of the metallic structures in the layout are dictated by the limits of the EBL process, corresponding to nanometric scales and the unit device scoped in this study is defined as a group of 100 µm-long parallelly placed NWs with varying pitches. Hence, the footprint of the key component of the device can be generically parametrized as a rectangle with a width of 100 µm and a length defined by the range of the NW array, which, from this point on, can be denoted as the fixed planar boundaries of the unit microfluidic interface for the device's sensitive region. Therefore, the governing geometrical constraints for the chip layouts and their consequent footprint requirements are mandated by the requirements of the microfluidic and electrical integration methods.

2.2. Microfluidics Integration

Since the mid-20th century, at the beginning of the silicon era, many technological advances, from polymerase chain reaction (PCR) to Human Genome Project (HGP), have reached their latest advances in co-evolution with the latest milestones in accompanying microfluidic systems [33]. Miniaturization of the systems gave scientists and engineers the capability to control small substances of interest in fluid environment. As the scale of boundaries of a liquid domain shrink, the ratio of inertial forces to viscous forces, described by Reynolds number (Re), decreases. The scale of most microfluidic applications incorporating channels of widths/heights ranging from 100 nm to 100 µm, Re is smaller than 2000, indicating that the regime is laminar and predictable through mathematical modelling, within computable uncertainties. In the meantime, the ratio of advective transport of molecules in a fluid to their diffusion coefficient, described by Péclet number (Pe), also reduces with downsizing. The reduction of the distance that molecules need to navigate in the fluidic domain to reach excitation for a chemical reaction and/or a physical interaction leads to faster reactions and consequently faster response times. On the other hand, the contribution of surface tension, the tendency of liquids to minimize their surface-to-air interface to reduce their free energy, and capillary forces become dominant over gravitational forces. Therefore, the characteristics of fluid-

surface interactions gain importance in integration of microfluidics.

In this study, several approaches utilizing PDMS and SU-8 materials were followed to confine analytes on the sensing region of the chip. Microfluidic channels of various sizes (width, length, depth), fluidic connection schemes through different inlet/outlet openings reservoir geometries were designed and fabricated. PDMS microchannels were created by producing mold structures as replicas of microfluidic channels by both lithographically patterned SU-8 molding and maskless lithography techniques. The produced PDMS microfluidic channels were bonded to the biosensor chips following oxygen plasma treatment. In addition, to achieve reversible sealing of microfluidic channels on chips, mechanical fasteners were designed and additively manufactured by using Formlabs Form 3+ model SLA type 3D printer. Finally, SU-8 itself is employed as the structural material of an open channel.

2.2.1. Microchannel Design

From a design perspective, the duty of the microfluidic channel is to confine a liquid substance to a certain volume, so that it can interact with the device. From an application perspective, the ideal case is when a device interacts with and/or responses to every single object of interest (a particle, cell, or a molecule). Therefore, the desired sample volume in interaction with the device depends on the application. For instance, microreactors developed for chemical syntheses aim smaller and densely arranged functional structures within a chamber to increase reaction rates, whereas they may be targeting production rates in higher volumes, unavoidably mandating higher dimensioning. On the other hand, for the most biomarker detection cases, the goal is to achieve detection with the smallest applicable specimen taken from the patient. Hence, the basic dimensioning of the microfluidic interface is of high importance.

The length of NWs corresponds to the width of the unit sensitive region to be interfaced with the analyte in microfluidic form, shortly denoted as the channel width. For a closed channel arrangement, the amount of the confined analyte is limited by the depth of the channel. Since the sensor considered in this study is a planar device with negligible thickness compared to the channel depth, the possibility of analyte-sensor interaction reduces with vertically increasing channel sizes, with respect to the sizes of substance to be detected. On the other hand, reduction in hydraulic diameter leads to tremendous

pressure drops throughout the channel [34], arising the requirement of a pumping agent to deliver the liquid. At this point, nature leaves us with the question of how much analyte we need in interaction with the sensing element. Answering to this question requires an application-oriented and iterative approach, starting from proof of detection capability of the sensor, followed by determination of LoD through series of experiments with systematically diluted analytes, and -if unknown- quantification of the substance in the real-life samples. As this question finds an answer, the minimum sample volume requirement is finally determined. Channel dimensioning and method of sample deployment strongly depends on this quantity. Inlet of a comparably low volume sample with respect to the sensing region is relatively easy, as long as wetting of that area by the analyte is ensured, whereas higher sample volume requirement with respect to the channel width necessitates continuous flow of analyte over the sensor until sufficient number of interactions occur for a meaningful signal to be generated for an assay. Hence, the first step of the general strategy is to minimize that amount by increasing sensitivity through sensor design optimization to avoid additional complexity of pumping mechanisms.

For the sake of generalization, we used a common SU-8 3050 resist, by which structural thicknesses from 35- to 115µm are available for spin speeds between 1000- and 4000-rpms [35]. The channel depth is designed as 50µm, deliberately selected at a value close to the lower limits of our resist to reduce non-interactive analyte, but at the same time not the lowest depth, to avoid pressure-drops and clogging. The channel widths are designed slightly narrower than the faithfully fixed NW lengths to ensure occurrence of sensor-functionalization and subsequent analyte-sensor interaction only on the sensitive nanostructures upon alignment and bonding; in other words, to passivate insensitive parts of the device form the fluidic contact. Finally, determination of the length concludes the interior design of the channel, which is directly related to NW arrangement within a single device, the number and spacing of multiple devices interfaced to a microfluidic sample along a single rectangular duct. For a closed channel geometry, limitations in the longitudinal direction are mainly the sample volume, the allowable footprint on the substrate, and obviously the increasing pressure drop with increasing channel length.

Whether a single droplet or a continuous flow of a large volume, the liquid sample must be delivered from the macro-world to the designated region in micro-scale, through proper connection elements with relatively larger sizes, compared to the channel itself.

26

Several methods are followed to tackle this practical issue. For closed channels, inlet/exit openings can be drilled/punched and seamlessly connected to a reservoir through tubing or to port-type structures with an embedded reservoir, whereas for the case of an open channel, a simple well at the channel's entrance with sufficient volume for placing the sample by a pipette of proper size would be enough. By all means, the footprint appropriated for liquid inlet/exit needs to be taken into account together with the devices' connections that must be electrically accessible but isolated from fluidics at the same time, for the final layout arrangement within the possibly minimum substrate area. Based on these considerations, the first conceptual layout design created in CAD environment fits 9 devices along a microchannel confined in a triple inlet-triple exit PDMS microfluidic chip and contact pads for electrical manipulation and measurement, as presented in Figure *6*.
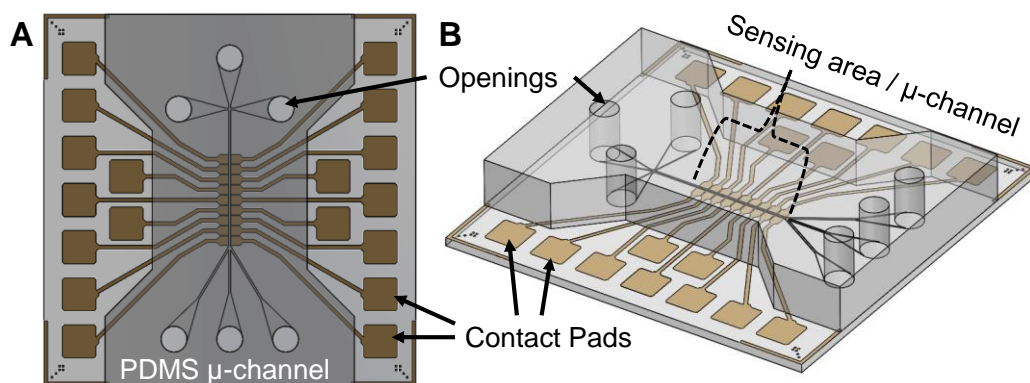
Figure 6. Conceptual design for integration of 9 devices on 2x2cm^2 substrate to PDMS microfluidic chip (A) top view, (B) isometric view.

2.2.2. PDMS Microchannel

Microfabricated Mold:

SU-8 molding is probably the most used technique for microchannel fabrication, as it exploits a good combination of advantageous features of SU-8 and silicon for casting PDMS. While SU-8 offers versatility in channel geometries as a negative tone photoresist with adjustable thicknesses, exceptional flatness of the single crystalline silicon wafer, or alternatively a glass wafer, conforms high adhesiveness for PDMS. Fabrication of the

SU-8 mold starts with wafer preparation step. The Si wafer is cleaned with acetone and isopropyl alcohol (IPA), then dried with nitrogen and by heating in an oven at 120°C for 10 minutes to ensure removal of all moisture for finer adhesion to the substrate. SU-8 is spun on the wafer at 3000 rpm for 50 seconds, which is followed by a soft baking step to solidify SU-8 layer by evaporation of its solvent. Then, the channel patterns are exposed by maskless UV lithography technique. The process continues with a post exposure baking step gradually at 60°C and 90°C to induce UV-exposed photoactive compounds for crosslinking, altering the exposed region's solubility in its developer. Afterwards the un-crosslinked regions are developed until no SU-8 residual remains. Finally, the mold is washed with IPA and dried with nitrogen gun (Figure 7).
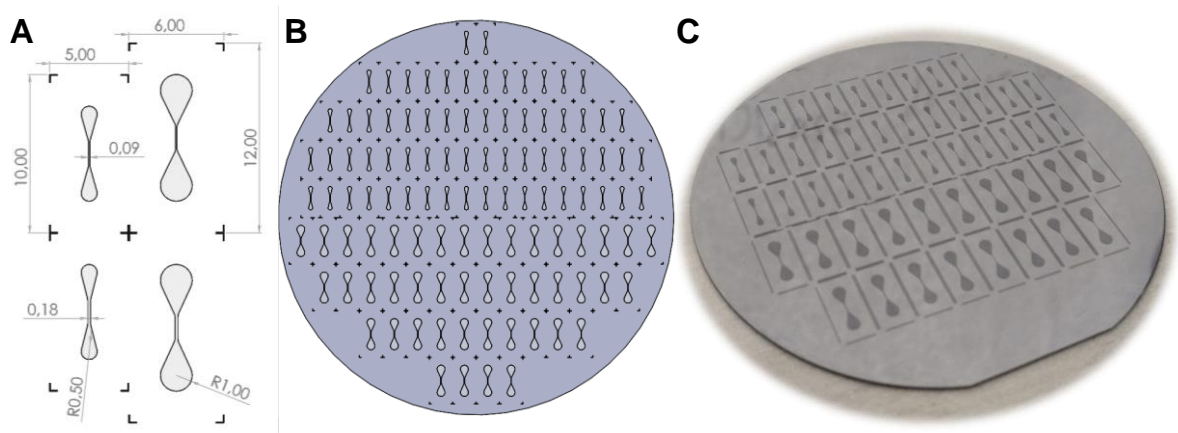
Figure 7. PDMS channel design studies based on SU-8 molding.
(A) Microfluidic chip designs based on channel width and inlet opening sizes. (B) Layout plan for multidevice mold on 4' wafer in CAD environment. (C) Produced SU-8 mold on Si wafer.

PDMS and curing agent are mixed to 10:1 ratio by weight. The mixture is degassed under vacuum in a desiccator to evacuate trapped air. Degassed PDMS is poured onto the mold and cured in a vacuum oven at 75°C for 2-3 hours, depending on the thickness. Then the cured PDMS is gently peeled off the mold, without contaminating the bonding surface and the channels. Biopsy punches with 1- and 2-mm diameters were used for the inlets and outlets, and cutting is done by a clean blade manually.

For bonding PDMS to glass substrate oxygen plasma treatment, corona discharge

treatment, and direct mechanical attachment methods were studied. O_2 plasma treatment of PDMS results in the removal of organic and hydrocarbon materials through chemical reactions with reactive oxygen species and ablation by energetic oxygen ions. This process introduces silanol (SiOH) groups, rendering the surface hydrophilic. When plasma-treated PDMS and glass surfaces come into contact, they form robust Si-O-Si covalent bonds, creating an irreversible water-tight seal for microchannel [36]. In this work, bonding quality by surface activation with O_2 pressures between 200-1000mTorr and RF power ranging from 10- to 30W were studied in a benchtop Harrick Plasma Cleaner.

As an alternative surface modification technique, corona treatment utilizes high-voltage, high-frequency electrical field applied to a metal electrode with a small air gap between the substrate, where the surrounding air molecules ionize and create plasma. The highly energized air molecules in the corona discharge contain reactive species such as ozone (O_3) and free radicals. These species react with the surface of the material to be treated, breaking, or modifying chemical bonds on the surface, similar to the O_2 plasma [37]. Upon treatment and bonding, strength of adhesion is subjectively assessed by a manual delamination test by vigorously detaching PDMS from glass. Corona treated chips performed stronger adhesion in most cases, however in the meantime they exhibited unbounded regions, while O_2 plasma resulted in uniform but weaker bonding. Based on the observations, corona treatment, however nonuniform, is simple and effective for strong adhesion, whereas bonding by O_2 plasma is achievable with a wide variety of parameters extensively studied in the literature [38], as well as by other methods [39].

On the other hand, regarding the application-specific materials, the effects of the surface activation process on the device must be eliminated, or at least minimized. When applied on the substrates with devices, corona treatment instantly burned the thin Au NWs, due to high electric fields and energetic radicals. On the other side, O_2 plasma operation, when generated at aforementioned pressure levels with higher RF powers than 30W, were observed to be either causing dramatic increases in the resistance by roughening or partially damaging, or complete breakage of NWs. Possible reasons are attributed to the oxide formation on the Au surfaces [40] acting as insulating layers impeding the electron transport; inclusion of additional roughness elements by grain boundary dislocations under reactive agents, and subsequent propagation of local nano-cracks are believed to be

29

causes altering resistance. Accordingly, the task turned into finding the parameters for adequate PDMS binding with lowest impact on NW resistance, which is achieved by gradually reducing O_2 pressure, RF power, and duration. To estimate the effect on the electrical characteristics of the NWs, resistance measurements were conducted before and after treatment, results are presented and discussed in the resistance measurement results section.

3D-Printed Mold:

Study by Bazaz et al. suggests another method which addresses utilization of rapid soft lithography by additively manufactured molds [41]. With this perspective, PDMS microchannels were obtained by the casting into microchannel molds that are stereo-lithographically (SLA) printed with a vertical resolution of 25 µm thick layers. Channels were then aligned and placed on the glass substrate containing gold nanowires without the need for clean room processes. Moreover, additive manufacturing provides flexibility in the creation of complex structures with vertically diversified features. Taking this advantage, the generated mold design embodies the reverse replica of a microchannel geometry with embedded conical inlet/exit reservoirs in conformation with commercial micropipettes for leakage-free injection of the analyte without requiring an additional coupling element. The amount of the sample to be injected is easily adjustable by resizing the reservoirs in the design phase, which is of high importance particularly when handling limited amount of valuable sample in microliter quantities.

Preparation of the PDMS and bonding are performed with the same protocol. A number of experiments conducted through this method have shown that yield of the products obtained by the 3D printed molds was not at the desired level due to the surface roughness tremendously reducing bonding quality. Moreover, the same roughness issue created difficulties in the demolding process albeit with the trial of using a mold release agent. Although it was possible to overcome these problems by employing an industrial-quality mold manufactured by injection molding of more suitable polymers or high precision machining of hard metals [33], it is far from the focus of this study in terms of time and cost. For this reason, despite the tangible capabilities provided by additive manufacturing methods, such as embedded chambers at the PDMS channel inlets, this technique has been abandoned. Despite that, the method is believed to have some potential to be

practical for studies involving channel structures that are larger in size or indifferent to the roughness element. The 3D printed mold, outcoming PDMS structures, results after delamination test showing stronger adhesion at high O_2 pressure plasma treatment with high RF power and strongest bonding with corona, together with the images of microfluidic chips upon bonding are presented in Figure *8*.
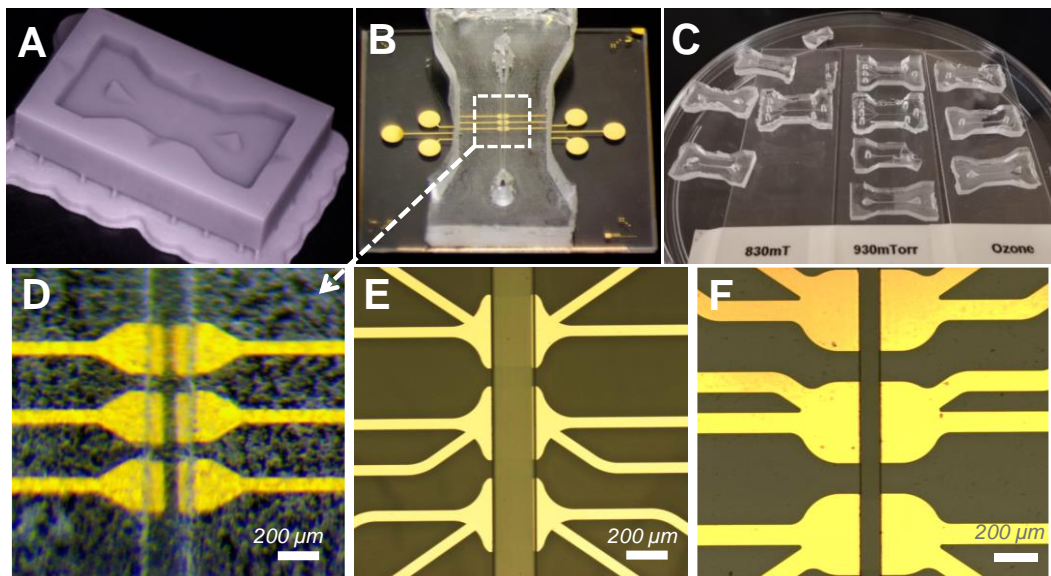
Figure 8. Images of studied microchannel structures.

(A) 3D-printed mold, (B) PDMS microfluidic chip made from A bonded to sumbstrate, (C) Sample delamination test results showing Results for PDMS microfluidic chips produced by (D) 3D printed mold, and (E) microfabricated mold. (F) SU-8 open channel.

2.2.3. SU-8 Microchannel

Utilization of SU-8 itself as a microfluidic channel structure can be advantageous over PDMS, depending on the application-specific requirements. As a rigid epoxy-based material, SU-8 exhibits much higher mechanical rigidity, higher temperature and chemical compatibility, higher resistance to degradation in long time, and lower gas permeability than PDMS. Thus, it can be used in devices that need to withstand pressure, elevated temperatures, aggressive chemicals, chemical reactions with gaseous products, or repeated use. Moreover, photolithographic patterning of the channel structures directly

on substrate eliminates highly labour-intensive molding, alignment, bonding steps; and most importantly the demand for enormous footprint required for PDMS bonding. With these considerations, the chip layout was redesigned to allow much more device placement on a unit substrate based on SU-8 open channel configuration, as shown in Figure 9. Electrical contact configurations are detailed in the electrical integration section.
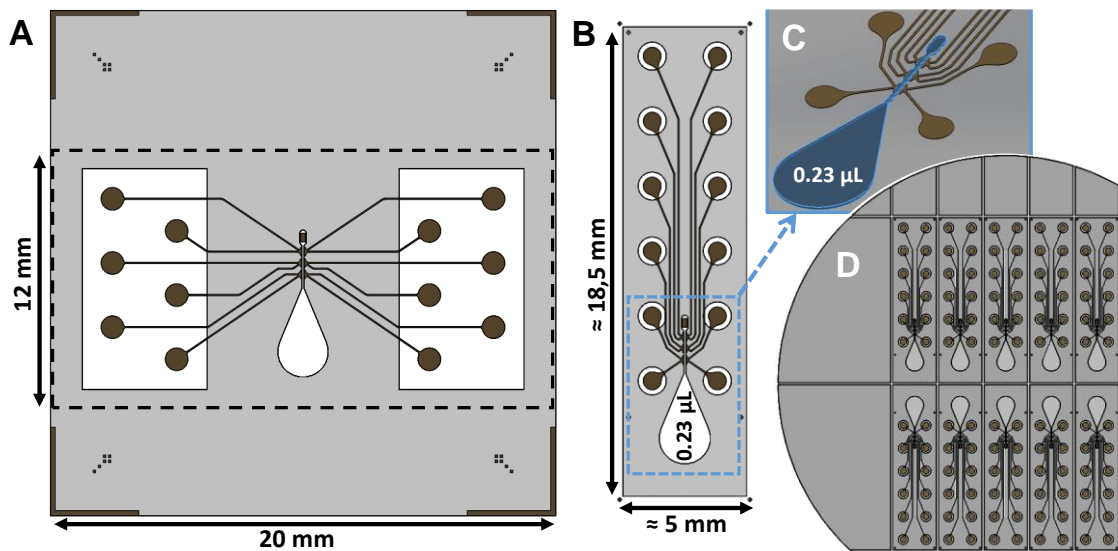
Figure 9. SU-8 channel design.

(A) on $2x2cm^2$ substrate in conformance with pogo-pin arrangement, (B) in densely packed formation. (C) Close up isometric view of the channel volume with 50 µm depth. (D) Arrangement of 10 chips, 3 per device on 2" wafer.

2.2.4. Microchannel Inlet/Outlet Interfacing

To finalize microfluidic integration, inlet/exit elements of microchannels need to be properly interfaced to the outer world. The requirements of the interfacing are predominantly mandated by the application-specific volumetric quantity of sample requirement. This section presents different connection elements and methods developed and produced for different sample quantities, based on the channel structures created in this study.

In contrast to plethora of studies pursuing for permanently sealed connections, this work

focuses on leakage-free and plug-in/out type reversible connections for closed PDMS channels [3]. For the openings made through 2mm diameter punch, delivery of the liquid to the confined sensing area is carried out through custom-designed structures, referred as port, and additively manufactured by SLA. The architecture of the port mainly contains a reservoir cavity with two vertical openings. The inlet is a hollow, right cylindrical protrusion on top for slip-on fitting silicone tubing, whereas the outlet at the bottom is designed as a special plug with a gradual dilation, starting with a smaller diameter at the tip to allow for easy insertion to channel inlet, which is mildly increasing to a larger diameter than the punched opening towards the centre for frictional sealing, and a negative taper from the centre towards the neck to provide self-locking feature inside stretched PDMS hole. As the flow can be pumped from a larger reservoir through tubing, for instance by means of a syringe pump, the port itself can also be employed as an elevated reservoir for feeding a slow capillary flow assisted by a small hydrostatic pressure until the total backpressure counterbalances. Utilization of the same plug geometry can be diversified as a direct tubing connection without an intermediate reservoir, or as a frictional fitting for conventional micropipette tips. On the contrary, the resolution of the 3D printer was not suitable for sustaining frictional sealing with a reliably unclogged opening for the tiny ports produced for 1mm openings. Additionally, they mechanically failed during plugging-in/outs. Apart from these, direct injection by micropipette through 1 mm openings were observed to be inefficient due to unfitting tips, while the channels produced by 3D printed molds with specially designed embedded conical reservoirs sustained pressure-driven shots for repetitive plug-in and -outs. However as previously mentioned, the roughness issue overweighs these practical advantages. Designs based on PDMS microchannel interfacing methods are schematized in Figure 10.
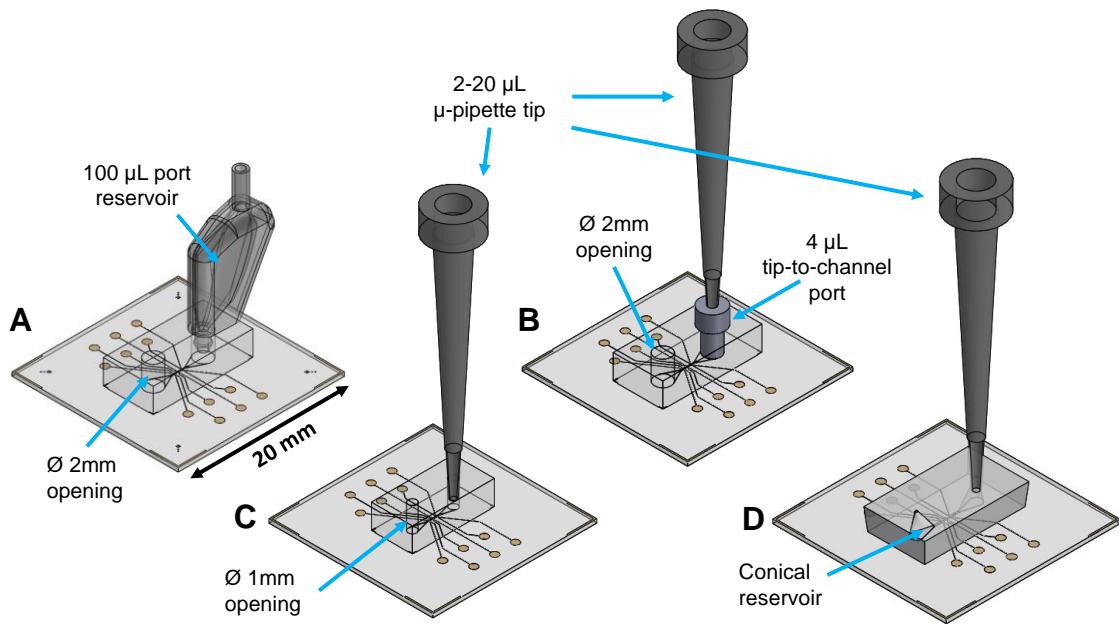
Figure 10. Schematics of studied PDMS microchannel interfacing methods. Implementation of port structures (A) with reservoir, (B) without reservoir. Direct μ-pipette injection to (C) Ø1mm punched opening, (D) embedded conical reservoir made from additively manufactured mold.

From the design perspective of this study, the area required for bonding PDMS stands as the bottleneck in lateral downsizing of the devices. Footprints can be reduced by utilizing very thin tubing, which requires some additional thickness for stable insertion. In terms of practicality, increasing thickness limits the magnification for optical imaging from top of the substrate, which is problematic especially when detection of weak optical signals is of concern and opaque substrate prevents inverted/confocal microscopy. On the other hand, although flexible nature of PDMS is suitable for cell applications, very thin PDMS structures are hard to handle, and deformations, however reversible, reduce repeatability because of handmade nature of integration process in laboratory environment.

Against PDMS, utilization of SU-8 as an open channel conforms densely spaced devices due to lithographical patterning, provided that an open well of proper size for placing the analyte. Similar to PDMS, hydrophobic nature of SU-8 necessitates some surface modification, such as oxygen plasma [42], to achieve interfacing the device with the fluid. Equivalently, conditions of performed plasma treatment must be harmless to the device, but at the same time sufficient for providing enough hydrophilicity to the channel to

overcome surface tension for wetting the sensitive region. Accordingly fabricated SU-8 channels and water contact angle measurement results are presented in Figure 11
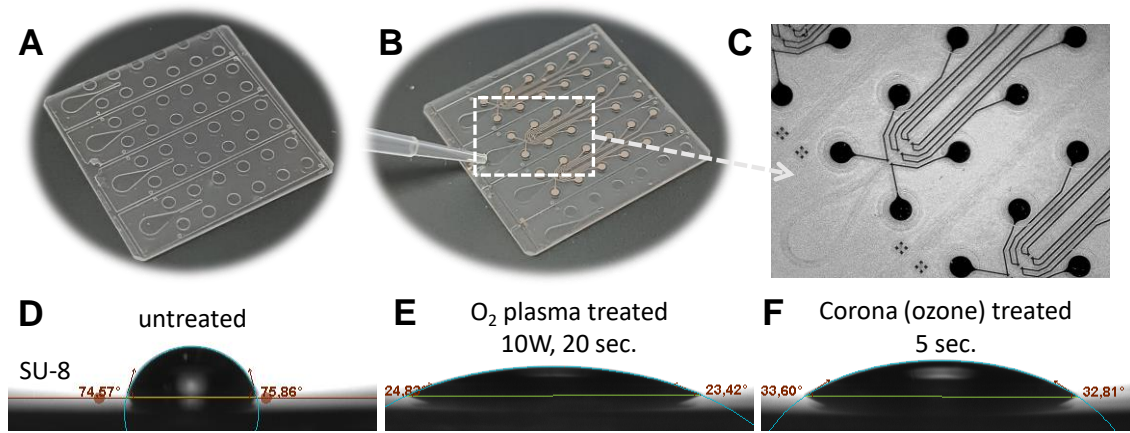
Figure 11. Images of SU-8 open channels

(A) on 2x2cm^2 bare glass substrate, (B) with devices and micropipette tip illustrating sample delivery, (C) close-up to well and devices; and water contact angle measurement results for (D) untreated, (E) O$_2$ plasma treated, and (F) corona treated SU-8 spun and baked on glass.

In contrast to permanently bonded closed channel configuration, open channel enables repetitive surface treatments, sample analyses, and can even sustain reusability upon proper cleaning and re-treatment. It is easier to reach to device in an open microchannel, making it prone to contamination. To avoid contamination while keeping the device more accessible for several purposes, such as effective washing of non-specific portion of an analyte after a test, which is hard to achieve by laminar flow through the microchannel. Washing may even be impossible for the cases where the subject to be washed shows low solubility. To address this issue, a magnetic holder is designed to obtain a reversibly sealed closed channel and electrical contact at the same time, as detailed in Section 3.3.1. It is important to note that the selection of the microfluidic channel integration method heavily depends on the application-specific considerations. If the analyte of concern is susceptible to open air contamination, such as rare aerosols, freely roaming enzymes or bacteria, practical advantages of an open channel may only become meaningful under a biological grade fume hood or in cleanroom environments. Table 1. summarizes different microfluidic approaches, based on closed PDMS- and open SU-8 microchannels.

Table 1. Comparison of PDMS & SU-8 channels

PDMS		SU-8
Channel Features		
Closed		**Open**
No sample contamination		Contamination possible
No evaporation:		Solvent evaporation:
Analyte is confined, no variation concentration		Analyte concentration may change in time.
Flow is prone to interruptions:		Flow does not get stuck easily.
Bubble formation, sample agglomeration, trapped particles		Interruptions can be washed away. Bubbles freely evacuate.
Min. analyte vol.: 3 µL		Analyte vol. limited by the µ-pipette: min. 0.2 µL
Device Footprint		
LARGE		Small
Fabrication & Integration		
SU-8 Mold	**3D-printed Mold**	Spin-coating followed by baking steps. Needs to be optimized to obtain a **stress-free** SU-8
Hard to cut out, PDMS thickness not repeatable	Lower resolution, wider channel size dimensions	
Alignment required for each chip: hard and time consuming		Regular mask alignment for whole wafer at once, followed by lithography
Bonding requires surface treatment, effective on baseline resistance		Surface treatment required for hydrophilicity, effective on baseline resistance

3.   METHODOLOGY FOR ELECTRICAL INTERFACING

Among various sensing approaches, direct electrical measurement is advantageous for label-free detection and point-of-care analysis through integrated electronic readout circuits. To achieve this, efficient fabrication of biosensors with nanoscale features and their integration to electrical readout through microscale interfaces is essential. However, prerequisite for reliable sensing is a reliable characterization process. This chapter will focus on the effort put into electrical integration of a generic device for achieving repeatable measurements, based on the example of nanowires.

3.1.   Electrical Integration

Commercial source/measure units (SMUs) are widely used instruments for conducting current versus voltage (IV) measurements across various fields for testing semiconductors, active/passive components, general electronic devices, and material characterization. In laboratory environment, SMUs are commonly interfaced to the measurand by means of a probe station, where the sample is positioned on a holder, on which specialized probes, such as a tungsten needle fastened to a screw-driven positioner, are used to make precise contact with the chip's contact pads or terminals. Probes and/or their holders can be spring-loaded to ensure consistent contact pressure and transmission of voltage and current signals to the SMU is made preferably through triaxial cables with proper guarding and shielding to minimize external interference and capacitive noise. When measuring an arbitrary resistor, this type of hardware is competent in accuracy, precision, and repeatability, provided that the contact between the probe and the

measurand is intact. However, the primary practical challenge encountered in establishing contact between a pointy tungsten object and an ultrathin physical vapor deposition (PVD) metal layer resides in its susceptibility to puncturing or scratching, permanently damaging the pad and making it impossible to repeat measurements from the same point on the pad. Secondarily, random vibrations are observed to be a source of noisy outputs stemming from the motion of the needle relative to the pad under frictional contact. Lower vibrational noise requires harder thrust force whereas harder thrust delivers more damage to the metal. One method to overcome this contradiction is to increase pad side metal thickness either by deposition or electroplating, so that the overall impact of penetration throughout the measurand become tolerable. Additional processes may, however, introduce risk of contamination and residual stresses that lead to changes in the character of the original sample. Another method would be wire-bonding of chip level pads to a board level circuitry, which is then robustly connected to a testing instrument or if possible, the complete measurement instrument itself can be constructed on the PCB. This method mostly eliminates the indeterministic contact resistance issue through seamless weldment and it can reduce the losses and noise to the levels of the PCB. However, designing a PCB as a connection interface and optimizing wire bonding parameters only for this purpose requires some effort that is indirectly related to the sensor/actuator parts characterization process. Thus, it is more feasible only after the device reaches a maturity level, where the key technological component on the chip is well characterized. The third solution is to introduce a less destructive contact with adequate vibrational isolation. To address this issue, wide variety of spring-loaded connectors are commonly used in industries such as electronics, telecommunications, automotive, medical devices, and aerospace [43].

A spring-loaded pin, also referred as pogo pin, is a simple electrical probe connector mechanism composed of a conductive pin (plunger) surrounded by a helical spring concentrically assembled inside a barrel. When the pin is pressed into the normal direction of a mating connector pad, the pin slides inside the barrel, compresses the spring, and applies a reaction force proportional to the spring's stiffness and compression displacement in the opposite direction. When the thrust force is removed, the spring pushes the pin back and releases the contact. This type of forced contact provides low electrical resistance and can support a wide range of current and signal requirements, making pogo pins suitable for both power [44] and data applications. Hence, a basic

assembly of an array of pogo pin connectors on a nonconductive fixture and a mating sample holder part is enough for convenient contact, which is necessary to perform electrical measurements, characterization of the device and determination of its physical limitations. Ad finem, what becomes measurable, can be improved.

Lead by the physical limitations of the key component, consecutive design parameters governing geometric, electrical, thermal, mechanical, and microfluidic boundary conditions of the complete system become manageable, enabling a holistic analogue circuitry design approach. Once the boundary conditions of each device, system, and sub-system are set, decision making cycle starts within frame of available fabrication and packaging capabilities together with economic considerations. With this approach, this study investigated electrical integration methods by systematic experiments. After each experiment set, an optimization cycle was sustained on both device layouts and experimental setup step by step to eliminate the possible causes of erroneous results and to improve the design by narrowing down the tolerances one at a time.

3.2. Readout Mechanism

This study started with measuring resistance of the nanowires fabricated by Şahin [32], first through large rectangular contact pads of the original design. For that purpose, Keysight B2902B Series Precision SMU is used with its probe station and Quick IV Measurement Software. The measurements are taken by SMU by contacting tungsten probes. Sharp tungsten needles scratch the pads and make repeatable measurements impossible. Therefore, the contact type is changed to the pogo pins with round probe tip, providing spherical contact rather than a point contact to minimize the damage through indentation of the tip to the thin metal film. Utilizing pogo pins introduces additional geometric constraints depending on the pin of choice. First, the sharpness of the contacting probe tip is the main indicator of applied pressure on the pad, which is inversely related to the radius of curvature of the round plunger tip. Secondly, the size of the barrel is the main constraint for the spacing between the pads, which consequently limits the minimum footprint of the device. Hence, the pogo pin for this application

should have a large plunger tip and a soft spring to avoid scratching, at the same time it should be barreled through the possibly smallest diameter to maximize the number of devices fitting in unit footprint.

For the designs created in this study, repeatability of the measurements is prioritized by selection of commercial round-tipped pogo-type connectors of approximately 1 mm pin diameter. To sustain modularity, the pogo pins are placed at (relatively large) intervals across a grid of 0.1 inches (2.54 mm), a common standard spacing for PCBs. Eventually, the selection of pins with known dimensions mostly concludes the minimum outer boundaries of the adjacent measurement setup for the maximum number of devices on a 2x2cm^2 glass substrate (Figure *12*). Accordingly, a substrate holder, I refer to as the base, and a pin holder, I named as the board, are designed. The base is a structure having a square slot dimensioned for matching in clearance fit with the substrate (slightly larger than the substrate) for positioning within acceptable tolerance for movement or misalignment and without getting stuck. Four through holes of 4 mm diameter serve for mounting the board by bolts. The through hole in the center with a diameter larger than the objective lens of our inverted microscope allows in-situ imaging, and the outer sizes of the base are again in clearance fit with the stage of the microscope. The board embodies two arrays of mounts for pins designed within press fitting tolerances, distantly located by a middle opening with the lateral sizes of PDMS for handling fluidics, and again four counterpart holes for assembly. Conceptual assembly of the integrated system design is presented in Figure *12*.

All mm-scale structural elements designed for this study are additively manufactured polymers, due to the advantage of rapid prototyping at low costs. Fused deposition modelling (FDM) is preferred for manufacturing relatively larger base part for superior structural rigidity and lower shrinkage rates at the expense of large clearances, whereas SLA (Formlabs Form 3+) is used to 3D-print the board to meet narrower tolerances required for tight fitting. The manufacturing steps and the unavoidable misalignment due to the relatively larger minimum tolerance range of FDM is compensated by the pad sizes in the chip design.
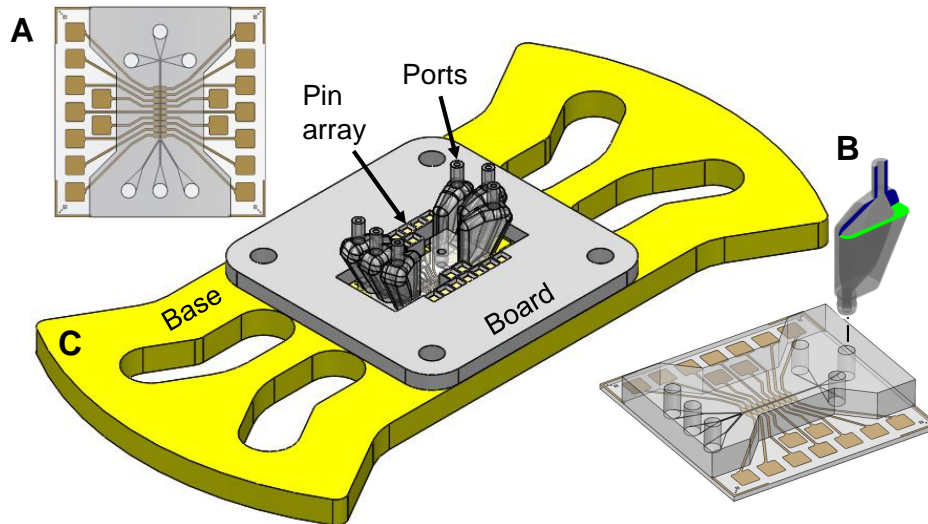
Figure 12. Integration concept of the chip

(A) Chip layout with microchannel, (B) Integration to fluidics by ports, and (C) packaging under the measurement system assembly.
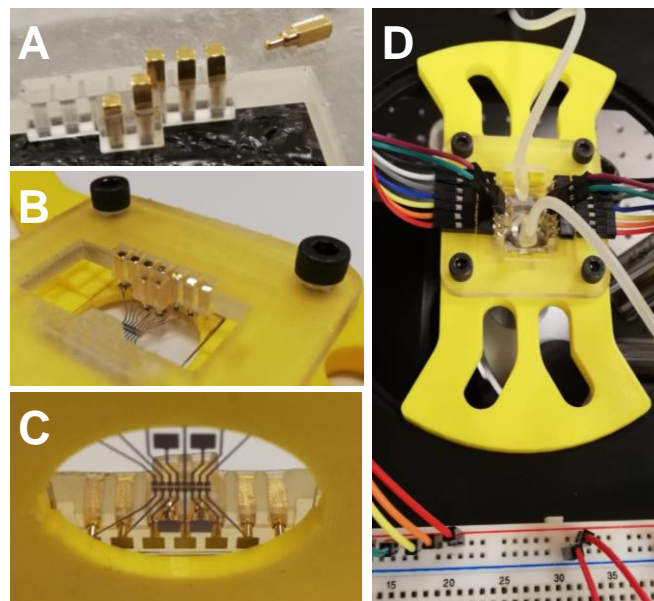
Figure 13. Assembly steps of the measurement setup.

(A) Press-fitting pogo-pins, (B) mating the base and the board. (C) Bottom view of the microscope window, (D) Image of the complete assembly placed at the inverted microscope stage.

At this point, one should keep in mind that the first aim was to achieve electrical characterization of the NWs fabricated by a single lift-of process., where the NW and pad

patterns are directly written by EBL, a heavy infrastructural element, whose utilization is costly in all terms (capital, operation, utility, time, energy, maintenance). Thus, another consideration is the reduction of EBL writing time. To address this issue, large rectangular pads are redesigned as circular structures connected to the smaller NW connection pads through narrower traces, as presented in Figure 14-A.

By integrating our custom-made probing mechanism to the SMU, measurements were conducted with a two-point probe resistance test configuration, the most common mechanism for IV measurements. In this setup, two probes, referred to as the source and the drain, are used to apply a known voltage across the device under test (DUT), and the resulting current flowing through the device is measured, as schematized in Figure 14 . The results, as discussed in the following section, showed a significant discrepancy between the devices with different number of equivalent NWs. The source of the issue is not a violation of the Ohm's law, but rather the inclusion of other non-negligible resistive elements in the 2-point probe technique [45], namely the contribution of the total lead resistance (R_{LEAD}) being comparably high -even dominant over low-resistance devices with large number of NWs- with respect to the resistance of DUT (R_{DUT}), where the devices connected to more distant pads through longer traces exhibit much higher resistances than the ones with shorter connection paths, but at the same time containing much fewer wires and proportionately higher R_{DUT}. While this practice justifies the necessity of minimizing R_{LEAD} to relatively negligible values respecting R_{DUT} by designing contact pads with incomparably large dimensions when measuring with the two-wire method, it also reveals the main issue of the method, that the read-out includes the cumulative effect of all resistive elements from the source to the drain, including pins, cables, and contact resistances.

Figure 14. Developed chip layout and integration arrangement for 2-point-probe measurement scheme.

(A) Second chip layout design for economized EBL writing. (B) Microfluidic integration and pogo-pin arrangement. (C) Assembly of measurement system, (D) Schematical representation of 2-point-probe resistance measurement method, taken from reference [45] (E) Projection of probing schematics for device measurement.

The limitations of 2-point probe measurement were overcome by employing 4-point probe, also referred as Kelvin probes, resistance measurement configuration. With this configuration, the test current (I) is forced through the test resistance (R) between two probes, the high force (HF) and the low force (LF). Two additional probes (high/low sense (HS/LS)) are used to measure the voltage drop across the sample. Connecting the HS and the LS as close as possible to the test resistance, for our case to the NWs, allows for more accurate measurement of the device's intrinsic electrical properties while eliminating the effects of contact resistance and lead resistance. Although some current may flow through the sense leads, it is negligible for practical purposes. Therefore, the measured voltage is essentially the same as the voltage across the test resistance. Henceforth, the layout is redesigned for four-wire probing approach, while preserving the adaptability to the measurement setup and microfluidics at the same time, as shown in Figure 15-A. Accordingly, each device demanding footprint for four connections (instead of two) strictly reduced the number of devices on our 2x2cm^2 substrate. The measurement setup is used as an intermediate vibration isolation element for providing secure contact with
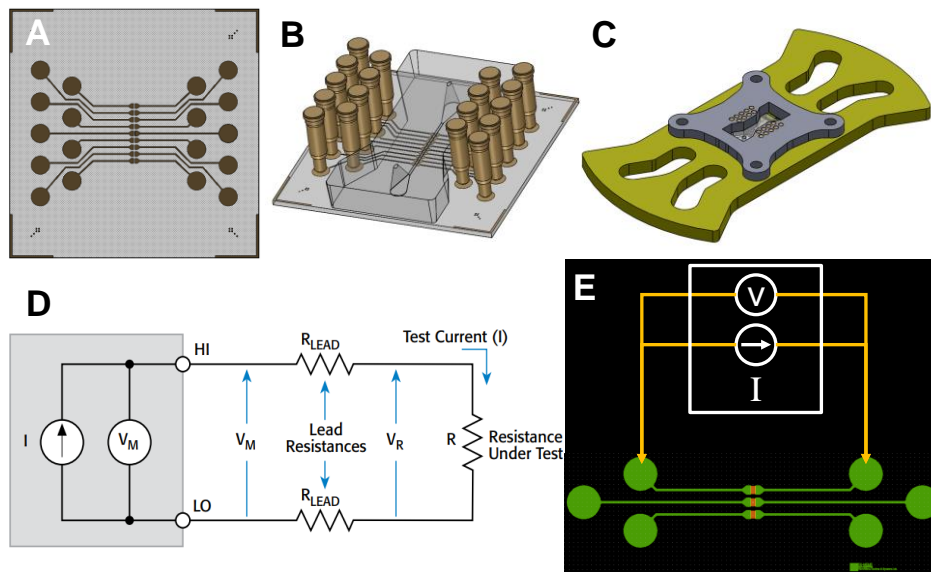
Cascade Microtech CP 4-point probe unit, as shown in Figure 15.
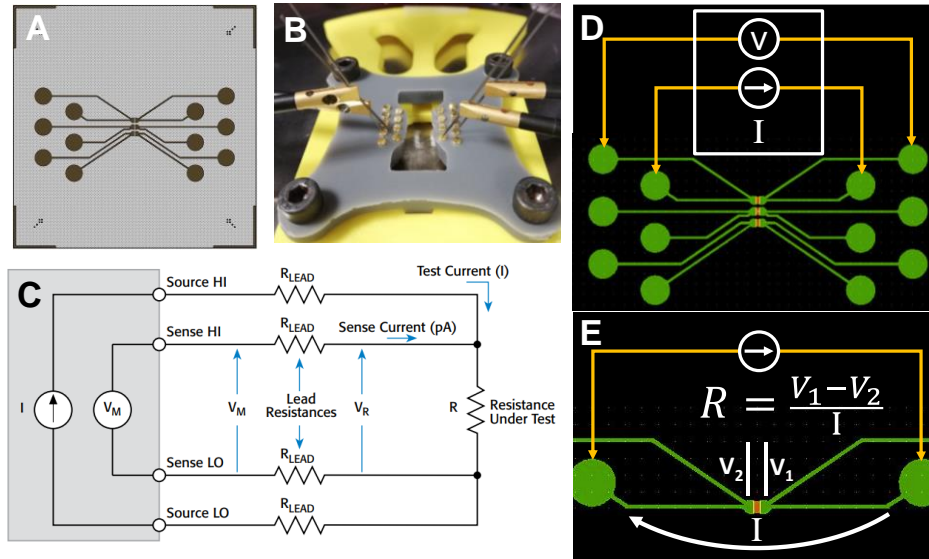
Figure 15. Developed chip layout and integration arrangement for 4-point-probe measurement scheme.

(A) Chip layout design for 4-wired probing. (B) The image of the measurement setup in use, connected to Cascade Microtech CP 4-point probe unit. (C) Schematical representation of 4-point-probe resistance measurement method, taken from [45] (D) Projection of probing schematics for device measurement and (E) calculation of resistance with the measured voltage drop.

3.3. System Level Integration

Along with the electrical measurements, design studies continued in parallel to densify structures as previously illustrated in Figure 9. As the chip design matures, the boundaries of the constitutive intermediate physical interface between the chip and the SMU or the readout PCB gains clarity. Moreover, the hands-on experience gained through measurements fed-back the valuable user experience forecast for exterior part design development with the aspects of functionality and ergonomics. With this concern, several conceptual designs are studied to achieve effective and user-friendly packaging & system level integration.

3.3.1. Magnetic Holder

A magnetic holder is designed to mechanically press untreated PDMS structures onto the substrate to obtain a reversibly sealed closed channel and electrical contact at the same time. This magnetic holder is an assembly of two main parts, the base and the board. In the same manner, the base has chip placement, and the board embodies the pogo pin array. Permanent neodymium magnets are placed in symmetrically distributed grooves to push the microfluidic chip and the pins down to the substrate, by means of magnets on base and board pulling each other. Finally, tapered protrusion at the board's bottom surface and the tapered groove in base counterpart adjacent to the chip placement builds up a self-alignment mechanism, eliminating bolting needs. A detailed description of the magnetic holder is presented in Figure 16.
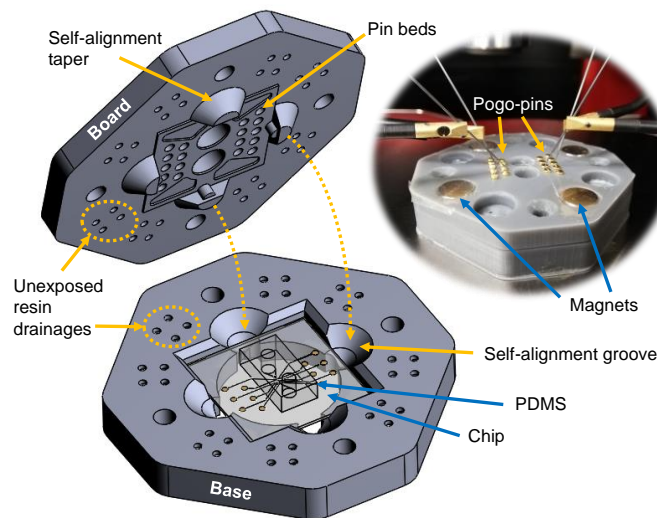
Figure 16. Description of the measurement setup with magnetic holder.

In this configuration, the same pin arrangement is used for testing the chips without changing the design; similarly, the setup can be used for any chip layout with the corresponding pad arrangement. One should note that the fixed geometry necessitates chips to be well-aligned to the substrate in the fabrication phase, to avoid misalignment. In case the alignment tolerances are rough, it should be compensated by dimensioning the pads. As a concluding remark to the method, the application's interference with the introduced magnetic field must be considered. Measuring the NW resistances by both setups, no distinguishable differences were observed.

3.3.2. Pogo-Pin Probe Clip

With the shrinking dimensions allowed by introduction of photo patternable SU-8 open channel configuration, requirement for the separation of H-F/S and L-F/S probes a distance by PDMS width becomes redundant. However, the contribution of the pogo pins due to the vibration isolating characteristics is still of interest. Therefore, a clip working with spring force is designed and 3D-printed. The main consideration by designing a clip mechanism is to calculate the length of the lever arm such that the moment created by the spring force at compressed distance equates the total moment with the opposite sign created by the compressed pogo pins at their working height. Alignment issues are solved for this method at the design phase of the mask for SU-8 patterning. For a known SU-8 thickness, dimensioning cylindrical openings slightly larger than the plunger diameter at the level of the contact constricts the lateral motion of the round tipped pogo pin. Provided that the radius of curvature of the pogo-pin tip is large enough and barrels, pads, and openings are concentrically aligned by design; the pins align themselves upon mild, manual, roughly aligned placement of the chip as presented in Figure 17.
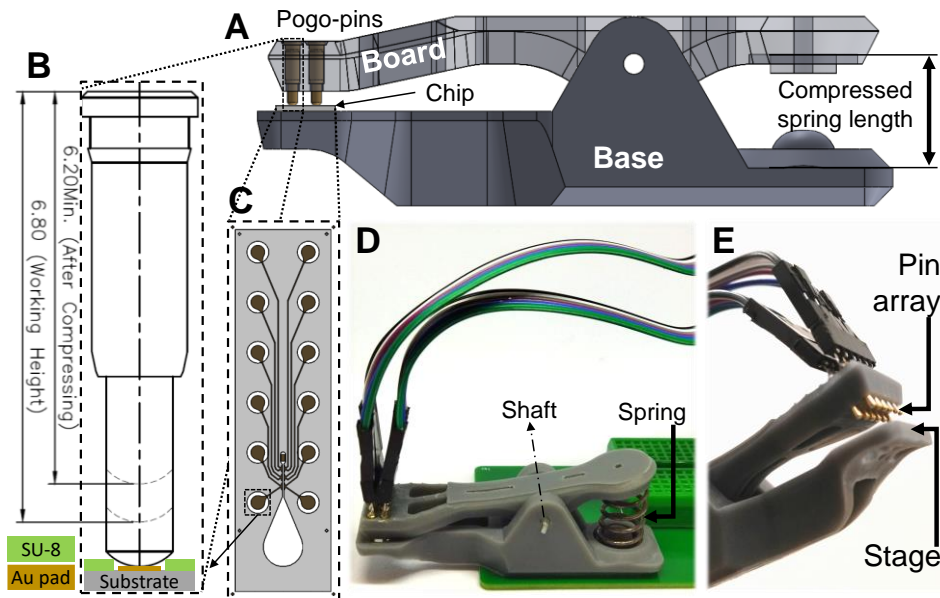
Figure 17. Description of the generated pogo-pin probe clip design:
(A) CAD image showing assembly of the base and the board parts. (B) Dimensions of the scoped pogo-pin and cross-section schematics of the self-aligning SU-8 opening for (C) the chip design with 3 devices based on SU-8 open channel configuration. (D) Image of the produced clip arrangement. (E) Close-up image of the pin array and the stage.

3.3.3. Readout PCB Packaging

The measurement system is integrated to the PCB designed in our research group in conformation with the same pogo-pin arrangement. Conceptually, the integrated measurement system turned into a hand-held device for PoC applications. The PCB design is generated for the 2-point-probe measurement principle, and its development is the subject of another study, therefore it will only be briefly described in this section.

The application of this device is to measure the resistor changes of the sensor and translate the changes to comprehensible results to be shared with users. The most significant aspect of this approach is a portable and easy-to-use device which not only visualizes the data immediately with an on-device LCD but also simultaneously upload the results to the cloud, so the data can be monitored on every location with access to internet. PCB designed for this service includes electronic parts to translate the sensor's resistance changes to voltage signals processed by a main microcontroller unit (MCU). Due to the low voltage excitation of the sensor, the design deals with very low input amplitude current levels, which are prone to noise. For higher accuracy of the resistance measurement, reducing the noise levels is the priority. First, using the Digital-to-Analog converter of the MCU, voltage levels of interest are applied to the sensor. For the NWs as a resistive-based sensor, the sensor's output is current. Using Ohm's law, the applied voltage over the sensor divided by the output current is the resistance value. However, the current output of the sensor can't be directly measured by any electronic device at a portable device level. Therefore, a conversion is required to convert the current to voltage levels to be measured by Analog-to-Digital converters and deliver the data to the MCU for further processing. The most effective approach for current to voltage conversion is to use a Transimpedance amplifier. The Transimpedance amplifier converts the input current in a closed-loop configuration with the desired gain. The Op-amp used in this configuration (OPA170, Texas Instrument) is a single-power and low power consumption component that eliminates the use of another negative power rail in the design and reduces the overall power consumption of the device.

As presented in Figure 18, the conceptual design for packaging of the system includes a base that covers the PCB, with a frontside slot where the chip is to be inserted upon

47

placing on its holder (which corresponds to chip packaging), and a fixer to push the chip holder against pogo pins to establish connection through one and a half screw pitch.
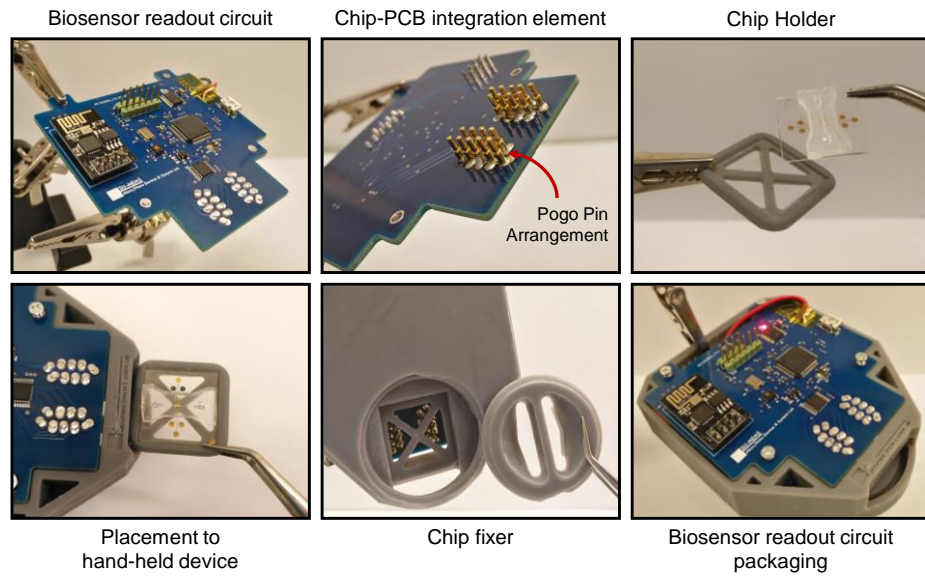
Figure 18. Readout PCB packaging.

4. FUNCTIONAL TESTING AND APPLICATION SCENARIOS

In this section, resistance measurements on the packaged sensor, ready to be connected to the microfluidic channel and readout circuit/measurement devices, are shown to demonstrate the functionality of the integration. As the base measurand, electrical resistance characteristics of NWs in different numbers and arrangements were inspected first by 2-point probe measurement and then by 4-point probe measurement techniques. The reliability and repeatability of the integration and measurement schemes were studied by repetitive measurements. Effects of surface treatment by O_2 plasma prior to PDMS bonding and subsequent SU-8 development were inspected, and the plasma conditions were optimized accordingly. Additionally, parameters for the SU-8 curing process are optimized based on resistance measurements indicating residual stresses due to uneven curing. Finally, a dielectrophoretic particle/cell separation application is simulated as a proof of functionality of the very first chip design and its integration concept.

4.1. Resistance Measurements
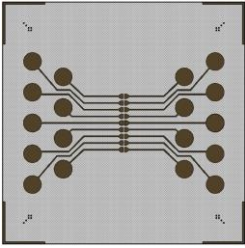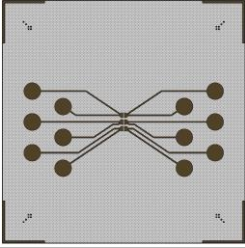
As Galileo Galilei suggests, "Measure what is measurable and make measurable what is not so." Development of a functional device first and foremost requires the precise measurement of the subject of application within acceptable tolerances. This study started with the electrical measurement of the subject of this study, NWs, by using Keysight B2902B Series Precision SMU with probe station, and Quick IV Measurement Software. The hardware stands out as a precision measurement unit, where the connection to the tungsten probe needles is made through triaxial cables providing extra shielding against electromagnetic interference. However, the bench that our probe station is located on was

49

relatively light in terms of mass, which is observed to be prone to random mechanical vibrations, that are further amplified by the thin features like needles at the end of the cables. This argument is easily proven by taking control measurements after adding mass on the table, or by slightly clicking at the table during measurement. Pressing the probes harder had only limited benefit in vibration isolation. On the other hand, damage caused by harder probe contact necessitated re-contact to an undamaged location on the pad for each measurement, resulting in different results. Although the pad width is more than hundred times the sum of the NWs', the differential length of manually adjusted contact points resulted in non-negligible resistance differences. To achieve precise measurement with this configuration, the pad resistance, irrespective of the probing point, needs to be negligibly small relative to the device, which is possible by thicker pads -requires additional fabrication process- or positionally fixing the probing mechanism within a tolerable range. Therefore, the first outcome of the resistance measurements was, as previously discussed in Section 3.2, pogo-pin arrangement to overcome the contact issue. The accuracy and repeatability of this method is experimented with repetitive measurements within 10 days. However, on the other hand, contribution of the lead resistances to the readout data being too much lead us to redesign the chip for 4-point-probe technique and the same test is conducted with the equivalent NW arrangements with 1-, 2-, and 5-µm pitch, as presented in Table 2. The results proved the functionality of the proposed system with round tipped plunger mechanism for repetitive measurements without damaging the pads of 25 nm thickness. Additionally, both methods showed good accuracy in resistance, but for very different nominal values.

4-point-probe measurement data directly corresponds to a voltage drop across the nanowires with small contribution of central NW contact regions, which is of high importance when detection by direct electrical measurement through a sensitive element is aimed. Although the accuracy of both data sets is satisfactory, contact resistances and metal traces are potential sources of noise, when other factors, such as thermal effects, come into consideration. This can be exemplified with the response of the whole device (NWs and traces combined) to the temperature changes due to different thermal expansion coefficients of the substrate and the metal being much larger than the thermal response of the small NW region. With this aspect, later measurements of this study were performed by 4-point probe method.

Table 2. Resistance measurement results for equivalent NW arrangements with 2- and 4-point probe measurement techniques. Sample NWs are arranged in the same area with varying spacings of 1-2-5 µm.

Measurements taken on 3rd, 5th,7th, and 10th day after lift-off.

Method	Chip Design:	NW Pitch [µm]:	1 (d3)	2 (d5)	3 (d7)	4 (d10)	Δ% d5-3	Δ% d7-5	Δ% d10-7
2-Point-Probe		1	103,22	103,11	103,47	102,92	-0,11	0,35	-0,53
		1	119,69	119,82	120,39	120,01	0,11	0,48	-0,31
		2	114,67	114,73	115,26	114,77	0,05	0,47	-0,43
		5	136,58	136,51	137,09	138,08	-0,05	0,42	0,72
		5	123,05	122,69	123,46	122,89	-0,29	0,63	-0,46
4-Point-Probe		1	4,45	4,40	4,39	4,37	-1,12	-0,23	-0,46
		1	5,48	5,45	5,45	5,44	-0,55	0,00	-0,18
		2	23,55	23,12	23,18	23,09	-1,83	0,26	-0,39
		5	23,55	23,12	23,18	23,09	-1,83	0,26	-0,39
		5	24,30	24,20	24,42	24,50	-0,41	0,91	0,33

After ensuring the reliability of the measurement, the effects of channel integration processes are assessed by sequential experiments. For the open channel configuration, the resistance measurements were performed on the chips after lift-off (bare NW resistance), after development and hard baking of SU-8 microchannel channel, and after application of O_2 plasma treatment which is followed by wetting test by placing a droplet to the open well by a micropipette. The measurement results related to SU-8 open channel are presented in Table 3. Similarly for the closed PDMS microchannels, bare resistance measurement is followed by after O_2 plasma treatment measurement, and after bonding measurement, additionally the effect of mechanical bonding of untreated PDMS is studied as well. The PDMS related sample measurements are presented in Table 4. Additionally, injection of fluidic sample based on the microchannel scheme, as discussed in Section 2.2.2, is studied after bonding.

Table 3. The measurement results for SU-8 open channel configuration

C: Chip number, D: Device number, L: NW length, T: NW thickness, and P: NW pitch.

C #	D #	L [μm]	T [nm]	P [μm]	Ω1 Bare	Ω2 SU-8	O2 Plasma Treatment	Ω 3 SU-8	ΩΔ% 2-1	ΩΔ% 3-2
	64	100	25	1	17,70	17,55		17,31	-0,85	-1,37
22	65	100	25	2	36,20	33,91		36,12	-6,33	6,52
	66	100	25	5	85,90	80,95	500 mTorr 20W 40s	109,75	-5,76	35,58
	67	200	25	1	24,05	22,77		22,50	-5,32	-1,19
23	68	200	25	2	49,70	45,88		45,95	-7,69	0,15
	69	200	25	5	208,80	182,86		180,90	-12,42	-1,07
	70	100	25	1	14,53	14,74		14,67	1,45	-0,47
24	71	100	25	2	27,13	26,67		26,55	-1,70	-0,45
	72	100	25	5	69,76	68,26	-	73,49	-2,15	7,66
	73	200	25	1	32,49	31,43		31,47	-3,26	0,13
25	74	200	25	2	62,43	61,88		61,00	-0,88	-1,42
	75	200	25	5	159,76	143,35		142,68	-10,27	-0,47

The decrease in resistance after processing SU-8 layer is an indicator of residual compressive stress, resulting from thermal non-uniformities during baking steps. To overcome this issue, the SU-8 process parameters are gradually revised. After some experiment sets, soft baking duration is decreased from 6 to 5 minutes, UV exposure time is reduced to 9 seconds, hard baking step is shortened to 15 minutes, and post baking times halved. While eliminating residual stress factor, plasma treatment became the only visible effect on resistance change. To eliminate that as well, governing parameters of the plasma treatment, RF power, pressure, and duration, gradually. At the end, surface is made hydrophilic, without altering the NW characteristics.

Table 4. The measurement results for PDMS microchannels

(The same notation is followed)

C #	D #	L [μm]	T [nm]	P [μm]	Ω1 Bare	O_2 Plasma Treatment	Ω2 PDMS	ΩΔ%
	76	200	25	1	25,97	500 mTorr 20 W 40 s	24,98	-3,81
26	77	200	25	2	49,41		47,70	-3,46
	78	200	25	5	122,40		119,33	-2,51
	79	200	25	1	75,13		80,78	7,52
27	80	200	25	2	137,60	-	154,03	11,94
	81	200	25	5	475,12		540,32	13,72
	82	100	25	1	18,44	500 mTorr 20 W 40 s	17,49	-5,15
28	83	100	25	2	33,72		32,82	-2,67
	84	100	25	5	80,76		79,86	-1,11

Plasma treatment and bonding of PDMS separately alter the resistance. Taking the cumulative effect into consideration, bonding by plasma treatment at 20W for 40 seconds decreased the NWs resistance, whereas mechanical bonding led to a remarkable increase. A comprehensive explanation for this result requires further investigation of plasma treatment effects. Apart from the plasma, some portion of the reason is believed to be the PDMS introducing compressive surface stress while covalently bonding to the glass substrate, leading to resistance decrease. On the contrary, mechanically compressing the PDMS towards the substrate leads to lateral expansion of the flexible material domain, introducing tensile stress to the substrate's surface elements. A detailed analysis could be performed to enwiden understanding of this event; however, it is beyond the scope of this study. Instead, applicability of milder plasma conditions to suffice bonding without altering the sensitive part is investigated. In the continuation of experiments, weaker plasma conditions were observed to result in ineffective bonding. Even if sealing was achieved, bonding strength reduced tremendously. Therefore, the effort is directed to increase sensitivity by reducing the number of NWs per device. The more sensitive NW arrangements were tested against both optimized microfluidic integration protocol and DC ranges to supply directly readable voltage measurement.

Among reviewed methods, performing a long set of systematical measurements with the help of our custom-made probing unit guided us to utilize SU-8 open channel structures subsequent to mild plasma treatment, which concludes this part of the study.

Table 5. The measurement results for 5-10-20 NWs with optimized SU-8 open channel configuration.

C #	D #	L [μm]	T [nm]	n [NWs]	Ω1 SU-8	O$_2$ Plasma Treatment	Ω2 SU-8	ΩΔ%
	169	100	25	10	362,00		358,00	-1,10
58	170	100	25	10	354,00		356,00	0,56
	171	100	25	20	170,00		170,00	0,00
	172	100	25	10	814,00		806,00	-0,98
59	173	100	25	10	718,00		718,00	0,00
	174	100	25	20	426,00		426,00	0,00
	175	100	25	10	1030,00		1032,00	0,19
60	176	100	25	10	596,00		596,00	0,00
	177	100	25	20	242,00	250 mTorr 10W 20s	242,00	0,00
	178	100	25	10	404,00		404,00	0,00
61	179	100	25	10	408,00		406,00	-0,49
	180	100	25	20	218,00		218,00	0,00
	181	100	25	5	1340,00		1360,00	1,49
62	182	100	25	10	666,00		666,00	0,00
	183	100	25	20	356,00		356,00	0,00
	184	100	25	5	1540,00		1540,00	0,00
63	185	100	25	10	834,00		834,00	0,00
	186	100	25	20	422,00		422,00	0,00

4.2. Application: Dielectrophoretic Cell/Particle Separation

In recent decades, studies on microfluidic applications have found interest in a large variety of areas. These have included, but not been limited to drug delivery, discovery and testing in pharmaceutics; in-vitro & in-vivo diagnostics in the health industry; diagnostics, packaging and testing in the food industry; DNA, protein and cell manipulation in biotechnology; lab-on-a-chip analytical chemistry; microreactors for chemical processing; control and measurement in process industries; soil, water and air measurements in environmental technologies; and injection, emission and particle control in the automobile industry. For numerous purposes, a great portion of these applications demand precise controllability on micro-/nano- sized inorganic particles, organic molecules, cells, viruses, proteins, nucleic acids, and other biological substances.

Among mechanical, magnetic, and optical methods, using electrical fields has numerous advantages such as high controllability, ease of operation, high efficiency, low cost, and low damage to sensitive biological particles [46]. Dielectrophoresis (DEP) is a method used for separation of suspended particles by means of polarization forces in a non-uniform electric field.

Dielectrophoresis (DEP) is a phenomenon in which a force is exerted on a dielectric particle when it is subjected to a non-uniform electric field. This force does not require the particle to be charged. All particles exhibit dielectrophoretic activity in the presence of electric fields. positive DEP (p-DEP) is the case where the polarizability of particle is greater than polarizability of the medium, hence particles are manipulated by forces acting in the direction of increasing electric field, whereas negative DEP (n-DEP) occurs when particles are manipulated by forces acting in the direction of decreasing electric field, due to polarizability of particles being less than polarizability of medium.
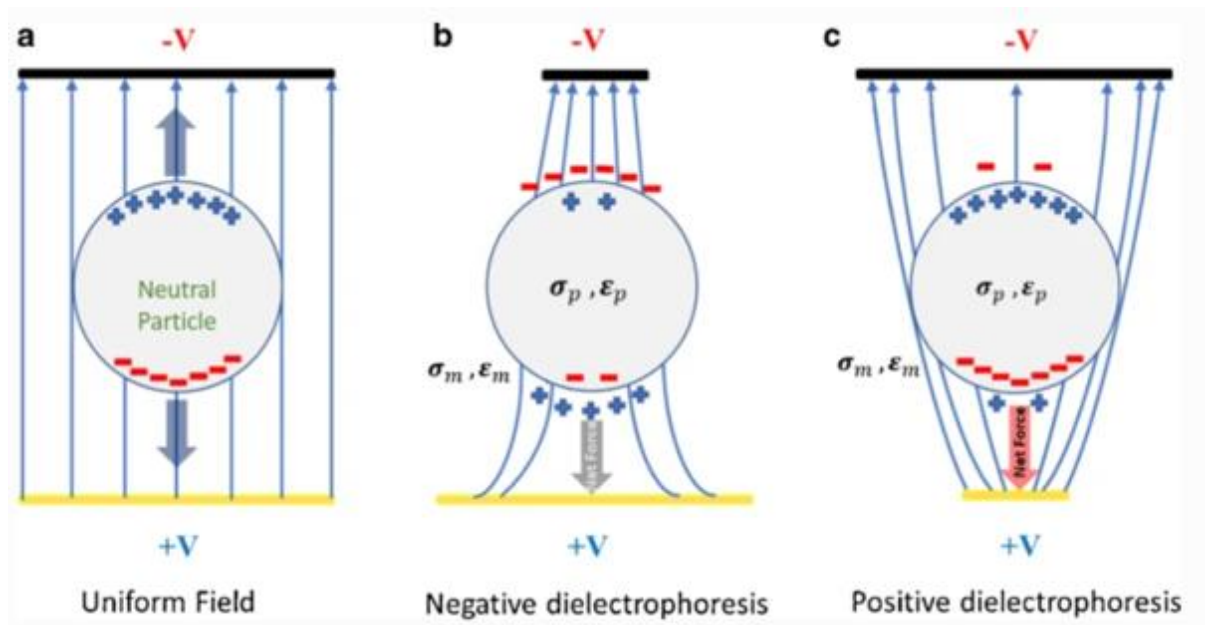

Figure 19. schematic showing the difference between a particle suspended within a parallel plate and a point-plane electrode system. When the particle polarizes, the interaction between the dipolar charges with the local electric field produces a force.
(a) No net forces. (b) Negative DEP net force (nDEP). (c) Positive DEP net force (pDEP)

The governing equation for DEP force exerted on an uncharged spherical dielectric particle is:

$$\mathbf{F}_{\text{DEP}} = 2\pi\varepsilon_m r^3 (k(\omega)) \, \nabla |\mathbf{E}|^2$$

(1)

where r is the radius of particle, ε_m is the permittivity of suspending medium, $|E|$ is the magnitude of the electric field, $k(\omega)$ is the Clausius-Mossotti (CM) factor,

$$k(\omega) = \frac{\varepsilon_p - \varepsilon_m}{\varepsilon_p + 2\varepsilon_m}$$

(2)

where ε_p is the particle permittivity. For an AC electric field, the equation for time average DEP force and CM factor becomes,

$$\mathbf{F}_{\text{DEP}}(t) = 2\pi\varepsilon_m r^3 \text{Real}[k(\omega)] \, \nabla |\mathbf{E}_{\text{rms}}|^2$$

(3)

$$k(\omega) = \frac{\varepsilon_p^*(\omega) - \varepsilon_m^*(\omega)}{\varepsilon_p^*(\omega) + 2\varepsilon_m^*(\omega)}$$

(4)

where ε_p^* and ε_m^* are complex permittivity of the particle and the medium where $\varepsilon\_^*$ is defined as,

$$\varepsilon^* = \varepsilon - j\frac{\sigma}{\omega}$$

(5)

and j is the unit imaginary number. For a uniform particle CM factor is obtained by combining equations (4) and (5)

$$k(\omega) = \frac{(\varepsilon_p - \varepsilon_m) - \frac{j}{\omega}(\sigma_p - \sigma_m)}{(\varepsilon_p + 2\varepsilon_m) - \frac{j}{\omega}(\sigma_p - 2\sigma_m)}$$

(6)

For the case of a cell that can be modelled as a spherical cytoplasm with complex permittivity of ε_{int}^*, surrounded by a cellular membrane with complex permittivity ε_{mem}^*, through thickness d, the effective permittivity of the cell, ε_{eff}^*, can be calculated according to single-shell model [47] as

$$\varepsilon_{eff}^* = \varepsilon_{mem}^* \frac{(\frac{r}{r-d})^3 + 2\frac{\varepsilon_{int}^* - \varepsilon_{mem}^*}{\varepsilon_{int}^* + 2\varepsilon_{mem}^*}}{(\frac{r}{r-d})^3 - \frac{\varepsilon_{int}^* - \varepsilon_{mem}^*}{\varepsilon_{int}^* + 2\varepsilon_{mem}^*}}$$

(7)

A greater ε_m^* than ε_p^* will result in positive $k(\omega)$ and causes attraction of cells towards the high electric field intensity by means of p-DEP whereas the opposite case is n-DEP. Real part of $k(\omega)$ depends on the frequency of the applied field and its value varies between -0.5 and 1. Other than the generated DEP force, viscous drag force acting on the particles/cells along the fluid flow according to the Stokes law:

$$F_{DRAG} = f.(v_f - v_p) \tag{8}$$

$f = 6\pi\eta r$ is the friction factor of particle, where η is the medium viscosity, vf and vp are the velocities of fluid and particle velocities, respectively. Considering the effect of gravity and Brownian motions within the scope of this study are relatively small, the governing equation for a particle based on Newton's second law reduces to

$$m\frac{dv}{dt} = F_{tot}$$
$$F_{tot} = F_{DEP} - F_{DRAG}$$

$$m\frac{dv}{dt} = F_{DEP} - f.(v_f - v_p) \tag{9}$$

where m is the mass of the particle, v is the fluid velocity and F_{tot} is the total force acting on the particle.

Finite element simulation model for DEP based separation techniques have been widely studied for diverse channel dimensions, electrode shapes and configurations, and cell/particle types [48]. With a conventional approach, design considerations depend on particle characteristics, and they restrict the geometry depending on the aim of application and once geometry is defined the electrical manipulations can be optimized accordingly. In essence, unsymmetrical electrodes in variety of shapes and configurations are preferred in most studies to achieve dielectrophoretic manipulation with utilization of electric field gradient in desired locations throughout a microfluidic channel. However, in this study, base design of the present microfluidic chip was used, without changing the electrode size, shape, and arrangement, which consist of two equally distant arrays of 9 rectangular electrodes symmetrically opposing each other. Unlike most of other studies involving dielectrophoretic manipulation, the electric field gradient is formed by unsymmetrical selection of electrodes to be biased in this study. In order to obtain the unsymmetrical electric field, the voltage is applied to the odd-numbered electrodes at one side and all the other electrodes were biased with the opposite sign of the same voltage in the simulation environment, and the result are observed.

2D representation for the predefined microfluidic channel and the electrode array geometries were constructed in COMSOL 5.5. The creeping flow module was used to define the fluid flow though the channel with an initial fluid velocity of 10 µm/s at the inlet. Electric fields were simulated in electric currents interface by applying potential to

the electrode domains. First, a stationary and a frequency domain study were run for the fluid velocity, pressure, and AC electric potential, respectively. Secondly, a time dependent study for particle trajectories was solved for the flow without DEP effects. Finally, particle trajectories including the DEP force was computed in the time dependent third study that uses the results from two prior studies to combine drag force and DEP force on particles throughout the flow.

The main parameters that effect the DEP force acting on a particle are radius of the particle, relative permittivity of the suspending medium, gradient of the electric field, and the CM factor of the particle that also includes the effect of conductivity and permittivity of the particle and the suspending medium. In this study, subjects of separation through the device were chosen as the ones that have been widely studied and whose dielectric properties are well known from the literature, such as polystyrene (PS) beads, as a standard particle widely used in the performance and quantitative evaluation of DEP systems [49]–[51], red blood cells (RBC) [47], [52], and thrombocytes (platelets) [53]. The thermophysical and electrical properties of particles and the fluid medium obtained from the literature are presented in Table 6. Properties of fluid & particles

Table 6. Properties of fluid & particles

Name	Properties of fluid and particles		
	Expression	*Value*	*Definition*
dp1	10[um]	2E-5 m	Particle diameter: PS
dp2	2.8[um]	2.8E-6 m	Particle diameter: platelets
dp3	3.29[um]	3.29E-6 m	Particle diameter: RBCs
epsilon_f	80	80	Fluid relative permittivity
epsilon_p1	2.5	2.5	Particle relative permittivity: PS
epsilon_p2	59	59	Particle relative permittivity: platelets
epsilon_p3	155	155	Particle relative permittivity: RBCs
epsilon_s2	4.44	4.44	Shell relative permittivity: platelets
epsilon_s3	10.67	10.67	Shell relative permittivity: RBCs
K_s	2e-9[S/m]	2E-9 S/m	surface conductivity
mu_f	1e-3[Pa*s]	0.001 Pa·s	Fluid dynamic viscosity
rho_12	1150[kg/m^3]	1150 kg/m³	Particle density (RBCs and platelets)
rho_f	1000[kg/m^3]	1000 kg/m³	Fluid density
rho_p	1062[kg/m^3]	1062 kg/m³	Particle density (PS)
sigma_bulk	1e-16[S/m]	1E-16 S/m	bulk conductivity PS
sigma_f	10[mS/m]	0.01 S/m	Fluid medium conductivity
sigma_p1	2*10^-4[S/m]	2E-4 S/m	Particle conductivity: PS
sigma_p2	0.31[S/m]	0.31 S/m	Particle conductivity: platelets
sigma_p3	0.73[S/m]	0.73 S/m	Particle conductivity: RBCs
sigma_s2	1e-6[S/m]	1E-6 S/m	Shell elec. cond.: platelets
sigma_s3	5.6e-5[S/m]	5.6E-5 S/m	Shell electrical conductivity: RBCs

Following the equations (6) and (7), the real part of CM factor for the particle properties in water medium were calculated in MATLAB. The real part of CM factor versus frequency plot up to 10 THz frequency is generated. It was observed that the platelets show two cross-over frequencies first from n-DEP to p-DEP around 180 kHz and p-DEP to n-DEP around 50 MHz, whereas RBC has only one cross-over frequency at 120 MHz from p- to n-DEP and PS shows n-DEP for all frequencies.

Plot of CM factor supplies the valuable advantage of being able to start with an educated guess of frequency range. From the plot, a range of useful frequencies around 180 kHz, where RBCs show p-DEP response, PS shows n-DEP and platelets show little or no response, which can be used to separate three particles throughout the channel. In the proposed design, based on the calculated CM factors, the optimum input frequency for a complete separation was searched with the help of the simulation. Results are given in Figure 20.
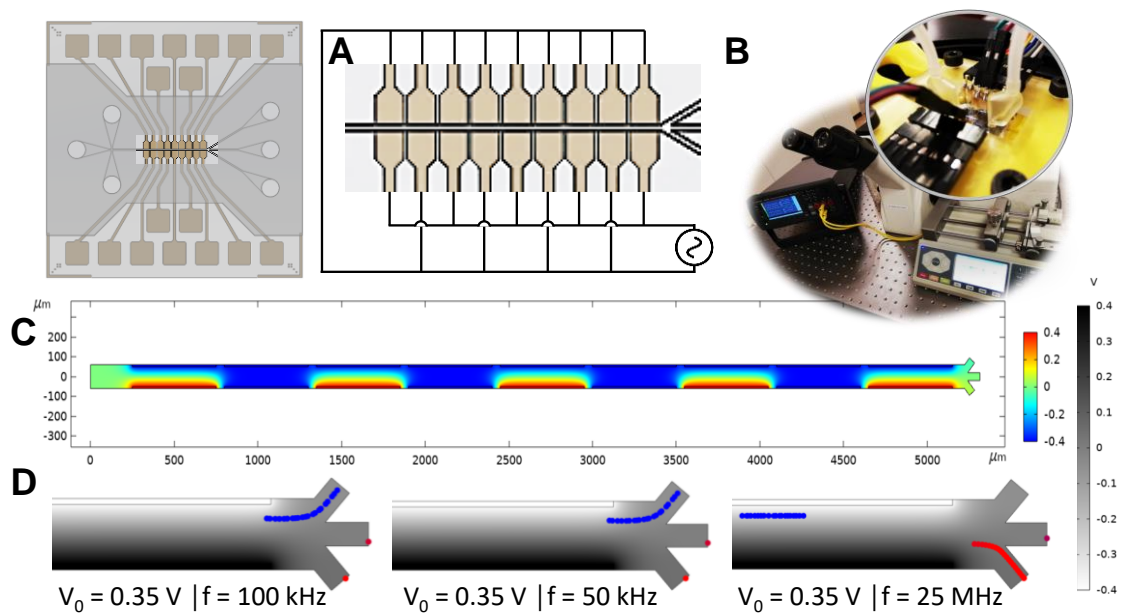

Figure 20. Presentation of the configuration and results of DEP studies:
(A) Simulation domain, (B) experimental setup, (C) Results of COMSOL electric field simulation, (D) Results showing the frequencies at which separation is achieved.

5. CONCLUSION

Microfluidic devices have ever-evolving applications in various fields such as biosensors. Electronic implementation on these microfluidic structures is providing opportunities for lab-on-a-chip devices. As reviewed in the first chapter, novel perspectives of biosensing applications exceedingly cover the materials or the applications within the concern of this study; however, a system-level integration requires allocation of intense amount of time and other resources to optimization of both structural and process-related parameters in correlation with material characteristics. Therefore, a systematical approach is required.

Prior to this study, considerations within the boundary conditions of an arbitrary device, system and subsystem have been discussed within a decision-making cycle taking the assessment of available manufacturing and packaging capabilities and economic considerations into account. With this approach, electrical integration methods are investigated in this study through systematic experiments. After each set of experiments, a step-by-step optimization cycle was carried out on both the device layouts and the experimental setup to eliminate potential causes of erroneous results and to improve the design by narrowing tolerances one by one.

At the beginning, the fabrication process of metallic nanowires, the key-component of this study, is reviewed. Centering nanowires of a constant length on the substrate, geometric boundaries of a generic system that interconnects electrical readout to microfluidics are discussed. Accordingly, channel geometry is defined based on the device level arrangement of the unit nanowires and chip level arrangement of devices. After defining volumetric boundaries of the central microfluidic domain to be interfaced with nanowires, fluid delivering concepts are designed based on the discussion of limiting material characteristics of PDMS and SU-8, the most common materials of microfluidic applications. Suggested designs are manufactured, and their functionality and practicality

are tested.

Along with microfluidics, integration methods to electrical readout are studied. Starting with a common, straightforward measurement scheme with regular, settled probing mechanism, the problems encountered in electrical measurements are discussed. To address these, a conceptual physical interface design that embodies pogo pins as interconnects between chip-level structures and outside measurement elements is proposed. The combination of geometrical constraints on the chip design introduced by selection of pogo pins and microfluidic integration method are discussed. Upon fabrication and utilization, the measurement setup is proven to be more efficient, effective, and reliable. Followingly, acquisitions by the proposed probing mechanism are reinforced with 4-point-probe measurement technique, providing refined resistivity characterization of nanowires by elimination of contact resistances and traces, at the expense of a doubled footprint. This method allowed for estimation of voltage drop just over the nanowire region, instead of all lead resistances combined.

Reinforced with a mechanically responsive set of nanowires which can be robustly connected to any desired measurement unit, effects of processes performed for integration of microfluidics are systematically tested. The results can be summarized as follows: First, corona treatment is highly destructive for thin metallic structures, therefore it is not an applicable surface activation method for this study. Secondly, for closed microchannels made by PDMS within the scoped dimensions, the required plasma irradiation for a strong bonding is found out to be altering nanowire characteristics. While a weak but leakage-free bonding with mild plasma conditions is applicable for relatively slow fluid flows, the bonding of the PDMS is observed to be effective on resistance. The effects are believed to be mostly stress-related, which is also expected to alter as the activated surface energy diminishes in time, but to be concise, the intrinsic effects at the active surface boundaries upon bonding by mild plasma treatment needs to be further investigated. On the other hand, while mechanical bonding is applicable as a robust method for fluid delivery, it introduces mechanical stress to substrate. Nonetheless, it requires repetition of alignment, which is somewhat troublesome, pointing out the need for an additional alignment tooling specialized for temporary PDMS bonding. Thirdly, the cumulative effects of fabrication parameters and surface activation by plasma treatment of open SU-8 channels are investigated. A recipe for fabrication of stress-free

SU-8 structures is proposed for the thickness of concern. Additionally, the plasma conditions to introduce hydrophilicity to SU-8 surfaces that allow fluid delivery without altering the nanowire resistances are defined. The generated resistance measurement data corresponding to the experimental conditions are reported. Finally, a conceptual study is performed in simulation environment that proves applicability of the proposed design for dielectrophoretic separation of various cells and/or particles.

To conclude, this work presents intellectual effort in a bottom-up design development approach for a device with the sensitive length of 100 µm, together with its electrical read-out & microfluidic integration. With the aim of producing an effective and feasible system in coherence with its application-specific physical boundaries, different methods were studied and practical results from several applications were presented. The difficulties due to the complexities of the system-level integration are addressed.

BIBLIOGRAPHY

[1]   E. Bassous, H. H. Taub, and L. Kuhn, "Ink jet printing nozzle arrays etched in silicon," *Appl. Phys. Lett.*, vol. 31, no. 2, pp. 135–137, 1977, doi: 10.1063/1.89587.

[2]   A. T. Woolley and R. A. Mathies, "Ultra-high-speed DNA fragment separations using microfabricated capillary array electrophoresis chips," *Proc. Natl. Acad. Sci. U. S. A.*, vol. 91, no. 24, pp. 11348–11352, 1994, doi: 10.1073/pnas.91.24.11348.

[3]   Y. Temiz, R. D. Lovchik, G. V. Kaigala, and E. Delamarche, "Lab-on-a-chip devices: How to close and plug the lab?," *Microelectron. Eng.*, vol. 132, pp. 156–175, 2015, doi: 10.1016/j.mee.2014.10.013.

[4]   P. L. Suryawanshi, S. P. Gumfekar, B. A. Bhanvase, S. H. Sonawane, and M. S. Pimplapure, "A review on microreactors: Reactor fabrication, design, and cutting-edge applications," *Chem. Eng. Sci.*, vol. 189, pp. 431–448, 2018, doi: 10.1016/j.ces.2018.03.026.

[5]   Duffy DC, McDonald JC, Schueller OJA, and Whitesides GM, "Rapid prototyping of microfluidic systems in poly(dimethylsiloxane)," *Anal. Chem.*, vol. 70, no. 23, pp. 4974–4984, 1998.

[6]   S. R. Quake, M. A. Unger, H. P. Chou, T. Thorsen, and A. Scherer, "Monolithic microfabricated valves and pumps by multilayer soft lithography," *Science (80-.)*, vol. 288, no. 5463, pp. 113–116, 2000.

[7]   H. Lorenz, M. Despont, N. Fahrni, J. Brugger, P. Vettiger, and P. Renaud, "High-aspect-ratio, ultrathick, negative-tone near-UV photoresist and its applications for MEMS," *Sensors Actuators, A Phys.*, vol. 64, no. 1, pp. 33–39, 1998, doi: 10.1016/S0924-4247(98)80055-1.

[8]   Market Data Forecast, "Global Lab On a Chip Market Size, Share, Trends, COVID-19 Impact & Growth Analysis Report – Industry Forecast (2023 to 2028)," 2023. https://www.marketdataforecast.com/market-reports/lab-on-a-chip-market

[9]   W. Jung, J. Han, J. W. Choi, and C. H. Ahn, "Point-of-care testing (POCT) diagnostic systems using microfluidic lab-on-a-chip technologies,"

Microelectron. Eng., vol. 132, pp. 46–57, 2015, doi: 10.1016/j.mee.2014.09.024.

[10] S. Smith, J. G. Korvink, D. Mager, and K. Land, "The potential of paper-based diagnostics to meet the ASSURED criteria," *RSC Adv.*, vol. 8, no. 59, pp. 34012–34034, 2018, doi: 10.1039/C8RA06132G.

[11] E. Mitri, G. Birarda, L. Vaccari, S. Kenig, M. Tormen, and G. Grenci, "SU-8 bonding protocol for the fabrication of microfluidic devices dedicated to FTIR microspectroscopy of live cells," *Lab Chip*, vol. 14, no. 1, pp. 210–218, 2014, doi: 10.1039/c3lc50878a.

[12] N. Azizipour, R. Avazpour, D. H. Rosenzweig, M. Sawan, and A. Ajji, "Evolution of biochip technology: A review from lab-on-a-chip to organ-on-a-chip," *Micromachines*, vol. 11, no. 6, pp. 1–15, 2020, doi: 10.3390/mi11060599.

[13] J. Aleman, T. Kilic, L. S. Mille, S. R. Shin, and Y. S. Zhang, "Microfluidic integration of regeneratable electrochemical affinity-based biosensors for continual monitoring of organ-on-a-chip devices," *Nat. Protoc.*, vol. 16, no. 5, pp. 2564–2593, 2021, doi: 10.1038/s41596-021-00511-7.

[14] A. Spanu, L. Martines, and A. Bonfiglio, "Interfacing cells with organic transistors: a review ofin vitroandin vivoapplications," *Lab Chip*, vol. 21, no. 5, pp. 795–820, 2021, doi: 10.1039/d0lc01007c.

[15] A. Maggi, H. Li, and J. R. Greer, "Three-dimensional nano-architected scaffolds with tunable stiffness for efficient bone tissue growth," *Acta Biomater.*, vol. 63, pp. 294–305, 2017, doi: 10.1016/j.actbio.2017.09.007.

[16] A. Teggert, H. Datta, and Z. Ali, "Biomarkers for point-of-care diagnosis of sepsis," *Micromachines*, vol. 11, no. 3, 2020, doi: 10.3390/mi11030286.

[17] A. Atala and J. G. Allickson, "Translational Regenerative Medicine," *Transl. Regen. Med.*, pp. 1–586, 2014, doi: 10.1016/C2012-0-06956-6.

[18] L. Parnetti *et al.*, "CSF and blood biomarkers for Parkinson's disease," *Lancet Neurol.*, vol. 18, no. 6, pp. 573–586, 2019, doi: 10.1016/S1474-4422(19)30024-9.

[19] O. G. Chavez-Pineda, R. Rodriguez-Moncayo, D. F. Cedillo-Alcantar, P. E. Guevara-Pantoja, J. U. Amador-Hernandez, and J. L. Garcia-Cordero, "Microfluidic systems for the analysis of blood-derived molecular biomarkers," *Electrophoresis*, vol. 43, no. 16–17, pp. 1667–1700, 2022, doi: 10.1002/elps.202200067.

[20] M. R. Kim and C. W. Kim, "Human blood plasma preparation for two-

dimensional gel electrophoresis," *J. Chromatogr. B Anal. Technol. Biomed. Life Sci.*, vol. 849, no. 1–2, pp. 203–210, 2007, doi: 10.1016/j.jchromb.2006.11.046.

[21] M. Nasir, M. H. Nawaz, U. Latif, M. Yaqub, A. Hayat, and A. Rahim, "An overview on enzyme-mimicking nanomaterials for use in electrochemical and optical assays," *Microchim. Acta*, vol. 184, no. 2, pp. 323–342, 2017, doi: 10.1007/s00604-016-2036-8.

[22] B. H. Villas, "Flow cytometry: an overview.," *Cell Vis.*, vol. 5, no. 1, pp. 56–61, 1998, doi: 10.1007/978-94-017-0623-0_1.

[23] S. Mastoridis, G. M. Bertolino, G. Whitehouse, F. Dazzi, A. Sanchez-Fueyo, and M. Martinez-Llordella, "Multiparametric analysis of circulating exosomes and other small extracellular vesicles by advanced imaging flow cytometry," *Front. Immunol.*, vol. 9, no. JUL, pp. 1–13, 2018, doi: 10.3389/fimmu.2018.01583.

[24] A. G. Theakstone *et al.*, "Fourier-transform infrared spectroscopy of biofluids: A practical approach," *Transl. Biophotonics*, vol. 3, no. 2, pp. 1–20, 2021, doi: 10.1002/tbio.202000025.

[25] D. L. Boyle, S. Rosengren, W. Bugbee, A. Kavanaugh, and G. S. Firestein, "Quantitative biomarker analysis of synovial gene expression by real-time PCR," *Arthritis Res. Ther.*, vol. 5, no. 6, 2003, doi: 10.1186/ar1004.

[26] S. Carrara, D. Sacchetto, M. A. Doucey, C. Baj-Rossi, G. De Micheli, and Y. Leblebici, "Memristive-biosensors: A new detection method by using nanofabricated memristors," *Sensors Actuators, B Chem.*, vol. 171–172, pp. 449–457, 2012, doi: 10.1016/j.snb.2012.04.089.

[27] R. Homsi, N. Al-Azzam, B. Mohammad, and A. Alazzam, "Memristive Biosensors for Cancer Biomarkers Detection: A Review," *IEEE Access*, vol. 11, pp. 19347–19361, 2023, doi: 10.1109/ACCESS.2023.3248683.

[28] M. A. Doucey and S. Carrara, "Nanowire Sensors in Cancer," *Trends Biotechnol.*, vol. 37, no. 1, pp. 86–99, 2019, doi: 10.1016/j.tibtech.2018.07.014.

[29] A. Vallero *et al.*, "Memristive Biosensors Integration with Microfluidic Platform," *IEEE Trans. Circuits Syst. I Regul. Pap.*, vol. 63, no. 12, pp. 2120–2127, 2016, doi: 10.1109/TCSI.2016.2608959.

[30] S. Naus, I. Tzouvadaki, P. E. Gaillardon, A. Biscontini, G. De Micheli, and S. Carrara, "An efficient electronic measurement interface for memristive biosensors," *Proc. - IEEE Int. Symp. Circuits Syst.*, 2017, doi: 10.1109/ISCAS.2017.8050685.

[31] I. Tzouvadaki, A. Tuoheti, G. De Micheli, D. Demarchi, and S. Carrara, "Portable Memristive Biosensing System as Effective Point-of-Care Device for Cancer Diagnostics," *Proc. - IEEE Int. Symp. Circuits Syst.*, vol. 2018-May, 2018, doi: 10.1109/ISCAS.2018.8351438.

[32] O. Sahin, "Optimization of Electron Beam Lithography and Lift-Off Process for Nanofabrication of Sub-50 Nm Gold Nanostructures," Sabanci University, 2019.

[33] N. Convery and N. Gadegaard, "30 Years of Microfluidics," *Micro Nano Eng.*, vol. 2, pp. 76–91, 2019, doi: 10.1016/j.mne.2019.01.003.

[34] H. Bruus, *Theoretical microfluidics*, vol. 45, no. 10. 2008. doi: 10.5860/choice.45-5602.

[35] KayakuAM, "SU-8 2000 Permanent Negative Epoxy Photoresist," *KAYAKU Advanced Materials, Inc.* pp. 1–6, 2020.

[36] L. Xiong, P. Chen, and Q. Zhou, "Adhesion promotion between PDMS and glass by oxygen plasma pre-treatment," *J. Adhes. Sci. Technol.*, vol. 28, no. 11, pp. 1046–1054, 2014, doi: 10.1080/01694243.2014.883774.

[37] M. Shahriar, J. Liu, H. Xu, Z. Zhang, and C. Xu, "Effects of Corona Treatment on Cellular Attachment and Morphology on Polydimethylsiloxane Micropillar Substrates," *Jom*, vol. 74, no. 9, pp. 3408–3418, 2022, doi: 10.1007/s11837-022-05378-x.

[38] K. H. Jung, D. G. Kim, and S. B. Jung, "Adhesion of PDMS substrates assisted by Plasma Graft Polymerization," *Surf. Interface Anal.*, vol. 48, no. 7, pp. 597–600, 2016, doi: 10.1002/sia.5985.

[39] A. Borók, K. Laboda, and A. Bonyár, "PDMS bonding technologies for microfluidic applications: A review," *Biosensors*, vol. 11, no. 8, 2021, doi: 10.3390/bios11080292.

[40] H. Ron and I. Rubinstein, "Alkanethiol Monolayers on Preoxidized Gold. Encapsulation of Gold Oxide under an Organic Monolayer," *Langmuir*, vol. 10, no. 12, pp. 4566–4573, 1994, doi: 10.1021/la00024a030.

[41] S. Razavi Bazaz *et al.*, "Rapid Softlithography Using 3D-Printed Molds," *Adv. Mater. Technol.*, vol. 4, no. 10, 2019, doi: 10.1002/admt.201900425.

[42] S. Kobayashi, E. Makino, T. Mineta, and T. Komatsuzaki, "Effects of microstructure geometry and plasma modification on wetting properties of SU-8 surfaces," *Microelectron. Eng.*, vol. 88, no. 8, pp. 1775–1778, 2011, doi: 10.1016/j.mee.2011.02.061.

[43] S. Bhattarai, H. Kim, S. H. Jung, and H. U. Oh, "Development of Pogo pin-based holding and release mechanism for deployable solar panel of CubeSat," *Int. J. Aerosp. Eng.*, vol. 2019, 2019, doi: 10.1155/2019/2580865.

[44] F. R. Lena *et al.*, "A novel sample holder for operando X-ray nanoscopy of perovskite solar cells," no. June, 2023.

[45] J. Janesch, "Two-wire vs. four-wire resistance measurements: which configuration makes sense for your application?," *Keithley kiadványa*, no. May. pp. 2–4, 2013.

[46] C. Qian *et al.*, "Dielectrophoresis for bioparticle manipulation," *Int. J. Mol. Sci.*, vol. 15, no. 10, pp. 18281–18309, 2014, doi: 10.3390/ijms151018281.

[47] Nurdan Erdem, Yagmur Yildizhan, and Meltem Elitas, "A Numerical Approach for Dielectrophoretic Characterization and Separation of Human Hematopoietic Cells," *Int. J. Eng. Res.*, vol. V6, no. 04, 2017, doi: 10.17577/ijertv6is040730.

[48] H. Zhang, H. Chang, and P. Neuzil, "DEP-on-a-chip: Dielectrophoresis applied to microfluidic platforms," *Micromachines*, vol. 10, no. 6, 2019, doi: 10.3390/mi10060423.

[49] Q. Chen and Y. J. Yuan, "A review of polystyrene bead manipulation by dielectrophoresis," *RSC Adv.*, vol. 9, no. 9, pp. 4963–4981, 2019, doi: 10.1039/c8ra09017c.

[50] Adam Rosenthal and Joel Voldman, "Dielectrophoretic Traps for Single-Particle Patterning," *Biophys. J.*, vol. 88, pp. 2193–2205, 2005.

[51] R. Deivasigamani, N. N. M. Maidin, M. F. M. R. Wee, M. A. Mohamed, and M. R. Buyong, "Dielectrophoresis prototypic polystyrene particle synchronization toward alive keratinocyte cells for rapid chronic wound healing," *Sensors*, vol. 21, no. 9, 2021, doi: 10.3390/s21093007.

[52] S. Park, Y. Zhang, T. H. Wang, and S. Yang, "Continuous dielectrophoretic bacterial separation and concentration from physiological media of high conductivity," *Lab Chip*, vol. 11, no. 17, pp. 2893–2900, 2011, doi: 10.1039/c1lc20307j.

[53] N. Piacentini, G. Mernier, R. Tornay, and P. Renaud, "Separation of platelets from other blood cells in continuous-flow by dielectrophoresis field-flow-fractionation," *Biomicrofluidics*, vol. 5, no. 3, 2011, doi: 10.1063/1.3640045.